Numerical Analysis of Vibratory Piling Effects on Offshore Heavy Lift Crane Dynamics

S.M.A. Hashemi

TU Delft
Huisman

Numerical Analysis of Vibratory Piling Effects on Offshore Heavy Lift Crane Dynamics

by

S.M.A. Hashemi

in partial fulfillment of the requirements for the degree of

Master of Science
in Mechanical Engineering

at the Mechanical Engineering Department of
Delft University of Technology

to be defended publicly on Wednesday October 29, 2025 at 12:00 PM.

Student number:	5901936	
MSc track:	Multi-Machine Engineering	
Report number:	2025.MME.9105	
Project duration:	February 1, 2025 - October 29, 2025	
Supervisor:	Ir. W. van den Bos	
Thesis committee:	Dr. J. Jovanova,	Committee Chair, ME Faculty
	Ir. W. van den Bos,	Committee member, ME Faculty
	Ir. T.B. (Thomas) Keesom,	Committee member, ME Faculty
	Ir. J. Los,	Company Supervisor, Huisman Equipment B.V.

This thesis report is a redacted version. Confidential and proprietary information has been removed.

TU Delft

Huisman

Preface

This thesis marks the conclusion of my graduation project, carried out at Huisman Equipment B.V., as part of my academic journey at Delft University of Technology. The project focused on vibration transfer and its effect on offshore cranes, and it provided me with a valuable opportunity to apply theoretical knowledge in a practical, industrial setting.

I would like to express my sincere gratitude to Dr. Jovana Jovanova for her guidance and for connecting me from TU Delft to a leading company in the design and manufacturing of offshore equipment such as Huisman. I am also deeply thankful to Ir. Wouter van den Bos for his continuous support, insightful feedback, and encouragement throughout the course of this project. His advice had a significant impact on my engineering mindset and personal development.

I am equally grateful to my company manager, Eric Romeijn, for giving me the opportunity to be part of a professional yet welcoming working environment at Huisman. A special thanks goes to my company supervisor, Ir. Jan Los, whose expertise, mentorship, and practical insights greatly enriched my understanding of the subject matter.

I would also like to extend my appreciation to all the engineers of the System Dynamics team, who were always supportive and never hesitated to guide me throughout this project. Special thanks to Sander Schot, whose knowledge in the field of research, along with his groundwork and reports, greatly helped me gain a deeper understanding of the topic.

This project has been a truly rewarding experience, allowing me to grow both professionally and personally. I am grateful for the knowledge I have gained and the collaboration I have enjoyed during this period.

Schiedam, October 2025

Ali Hashemi

AI Statement

In this report for the course ”Graduation Project ME54035”, I have used Generative AI tools to:

- Create the picture used in the cover.
- Improve the grammar, style, layout, and spelling of the text.

In all cases I have reviewed and corrected the work and remain fully responsible for the content of the report.

Company Background

This thesis has been carried out in collaboration between Delft University of Technology (TU Delft) and Huisman Equipment. The cooperation combines the academic expertise of TU Delft in structural dynamics and offshore engineering with Huisman's industrial experience in designing and fabricating advanced heavy lifting systems. This partnership created the opportunity to investigate an engineering challenge that is directly relevant to the offshore wind industry and to Huisman's product portfolio.

Huisman Equipment is an international company specialized in the design, fabrication, and servicing of heavy lifting and handling systems for offshore, renewable energy, and industrial applications. Among its most prominent products are large offshore cranes, which are essential for the installation of wind turbines and monopiles in offshore wind farms. With decades of experience and a reputation for pioneering engineering solutions, Huisman delivers equipment tailored to client-specific requirements, such as lifting capacity, radius, height, and operational conditions including vessel motions, wind, and temperature ranges.

Figure 1: Offshore Knuckle Boom Crane designed and manufactured by Huisman Equipment

In the offshore wind sector, Huisman's cranes are frequently deployed in monopile installation projects where vibratory piling equipment may be utilized. Because of the demanding operational environment and the long service life expected from such equipment, Huisman applies advanced engineering methods and predictive analyses to ensure the safety, durability, and performance of its offshore lifting solutions.

Summary

This thesis investigates vibration transmission during vibratory piling (VP) with a focus on risks to the lifting equipment. The work is motivated by incident reports and by the absence of field measurements on cranes during offshore operations. The study aims to identify resonance frequency(ies), quantify component displacements, determine forces in the hoist cable, and characterize how each component responds across the input frequency range. A secondary aim is to relate frequencies that favor pile penetration to potential risks for the crane.

A two stage modeling approach is adopted. First, the crane is generalized to a two dimensional (2D) form and converted to a one dimensional (1D) system of lumped masses and linear springs aligned vertically. The pedestal is idealized as fixed. Linear behavior and small displacements are assumed. Second, the monopile (MP) is modeled in Ansys with shell elements to capture flexible body behavior. A mode reduction retains only axial modes of the MP, since bending, torsion, and circumferential shell modes do not directly couple to the vertical vibration path that governs VP. Depth dependent stiffness and damping represent the soil at the toe. Hoist stiffness varies with depth through cable length.

The calculation method separates free and forced vibration. In free vibration, the system eigen-problem provides resonance frequency(ies) and mode shapes with the MP first treated as rigid. The axial flexible body natural frequency of the MP is then obtained from the shell model. In forced vibration, the harmonic response is computed to obtain frequency response functions and absolute displacement magnitudes for the components, as well as the hoist cable force.

Results show two frequency families that govern the response. The first family contains the system resonance frequency(ies) with a rigid MP. The second family contains the axial flexible body natural frequency of the MP. Modes 1, 2, and 4 are largely insensitive to MP flexibility. Mode 3 and the axial flexible body frequency depend strongly on the soil stiffness at the toe and shift with depth. Within the operational range of the vibratory/vibro hammer (VH), the fourth system resonance and the first axial flexible body frequency of the MP lie close together and can interchange order as depth changes.

The harmonic response clarifies component participation at key frequencies. Near Mode 3, motion concentrates in the exciter and MP and engages the soil stiffness most strongly. Near Mode 4, the lower block and bias mass dominate while the MP response is limited. At the axial flexible body frequency of the MP, the head and toe move in opposite directions with a near stationary point along the pile length, consistent with a fundamental axial mode. These behaviors explain the locations and amplitudes of the observed peaks.

A verification step compares boom tip response and hoist cable force between the simplified system and the full finite element (FE) crane. The first peak aligns in both models, supporting the validity of the simplified representation for global behavior. Differences at higher frequencies are traced to flexible crane substructures that the simplified model does not include. This comparison establishes where the simplified model is reliable and where detailed crane is more suitable for cranes structure fatigue study.

Mitigation is explored conceptually. Removing the hoist load path would eliminate force transmission into the boom, but this is often impractical. Introducing an isolator between the lifting equipment and the piling equipment is a more practical option. When tuned near the axial flexible body frequency of the MP and near the fourth system resonance, an isolator can reduce force transmission into the boom while preserving penetration performance.

The study concludes that frequencies that favor penetration can occur near frequencies that amplify responses in the lifting equipment. Managing this close proximity requires attention to frequency modes, awareness of depth effects through soil stiffness, hoist force fluctuations, and consideration of isola-

tion in the load path. The work provides a structured method to identify critical frequencies, quantify responses, and separate the roles of monopile flexibility and crane structure, while pointing to targeted measurements and modeling extensions that would complete a validated framework for decision making.

Contents

List of Abbreviations

1D one dimensional

2D two dimensional

DOF degree of freedom

DP dynamic positioning

FE finite element

FEA finite element analysis

FEM finite element method

FRF frequency response function

JUV jack-up vessel

LEC leg encircling crane

MP monopile

OMC offshore mast crane

SWL safe working load

TMC tub mounted crane

VH vibratory/vibro hammer

VP vibratory piling

List of Figures

List of Tables

1

Introduction

Offshore wind is scaling fast in both capacity and turbine size, driving heavier foundations and more demanding installation campaigns. Market outlooks and industry surveys highlight steep growth trajectories and widespread reliance on monopiles, which now commonly exceed 10 meters in diameter and 100 meters in length, with continued up-sizing expected as turbines grow (BOSLAN Ingeniería Consultoría, 2022, McCoy et al., 2024).

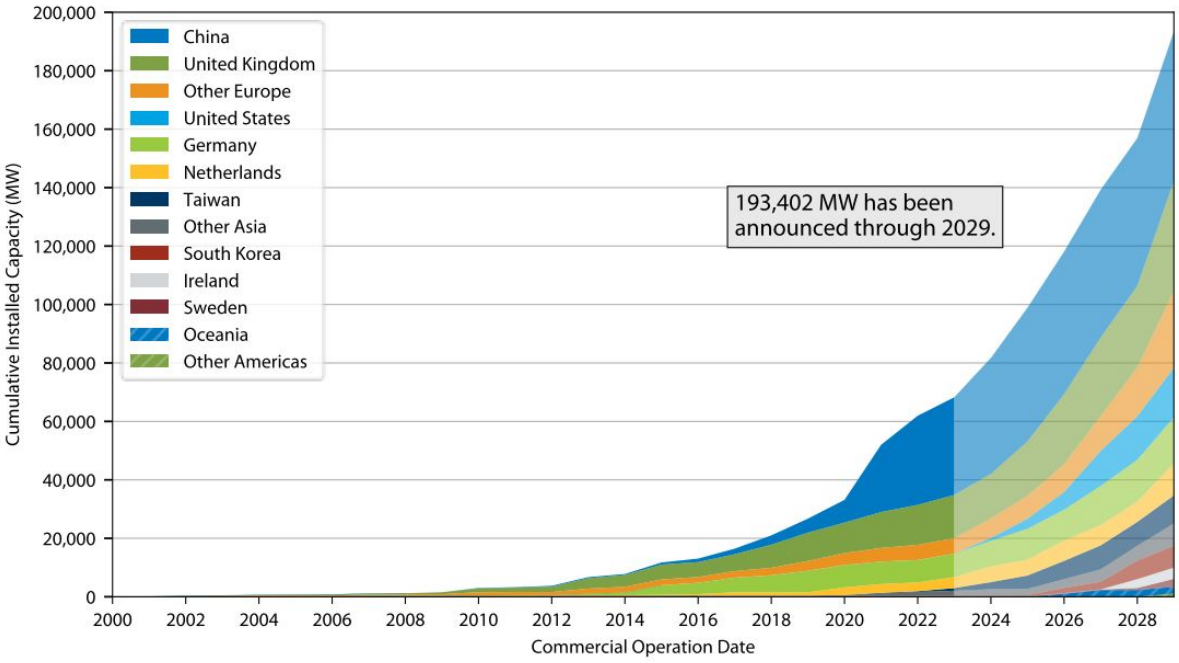

Figure 1.1: Estimated cumulative fixed-bottom and floating offshore wind capacity by country based on developer-announced commercial operational dates (McCoy et al., 2024)

Vibratory piling is increasingly attractive for these large foundations because it shortens installation time and, crucially, produces markedly lower peak underwater sound levels than impact hammering. Comparative reviews consistently report peak and single-strike levels for impact piling that exceed those from vibratory driving by 10–30 dB (or more), reducing marine noise risk and the mitigation burden (Seiche Ltd, 2021).

Yet, while vibratory methods can reduce environmental footprint, they also introduce high-frequency, continuous forcing into the lifting line and crane structure. Practitioners report perceptible vibrations at the operator cabin under certain conditions, but quantitative, system-level guidance on when and

how these inputs excite crane substructures is limited. A model-based frequency response approach can close this gap by identifying resonance families, clarifying component participation, and quantifying the transmitted loads that matter for operations and risk management. (Industry standards and project documentation emphasize managing dynamic effects in marine operations, but do not resolve the crane–pile–soil coupling central to vibratory piling) (Niu et al., 2023, Tsouvalas et al., n.d.).

1.1. Scope of Research

This study investigates vibration transmission during VP with emphasis on risks to the lifting equipment. The scope is limited to identifying resonance frequency(ies), mode shapes, displacement magnitudes of key components, the frequency response function, and the force in the hoist cable. The crane is represented by a generalized model reduced to a one dimensional system of lumped masses and linear springs aligned vertically. The pedestal is idealized as fixed. Linear behavior and small displacements are assumed. Damping is included only in the forced vibration analysis.

The MP is modeled separately in Ansys using a shell formulation to determine its flexible body behavior. A mode reduction retains only axial modes, since bending, torsion, and circumferential shell modes are not directly involved in the vertical transmission path considered in this work. Soil is represented at the toe by depth dependent stiffness and damping; hoist stiffness varies with depth through cable length.

Out of scope are detailed checks of allowable stresses, fatigue damage, weld design, and safety factors, as these are addressed in standard crane performance evaluations. Also excluded are vessel global motions, controller dynamics, rigging nonlinearity beyond the adopted stiffness representation, and comprehensive shaft resistance along the embedded pile length.

The analysis relies on project data provided by Huisman Equipment and on manufacturer information for the piling equipment. Results are presented for free vibration and harmonic response, and are compared where relevant to a full FE crane model to assess the representativeness of the simplified approach.

1.2. Research Questions

Main question

”What is the effect of vibratory piling on crane during mono pile installation using vessels?”

To be able to answer the main research question more effectively, the following sub-questions are defined. Answering these sub-questions will provide a clear understanding of the process, facilitating the approach to addressing the main research question.

Sub questions

1. How is vibration generated in vibratory pile driving equipment (vibro hammer)?
2. How is vibration transmitted throughout the system?
3. What are the posed risks of transmitted vibration to the equipment?

1.3. Structure of the Report

This report moves from context to methods to results, followed by solution proposal. For a quick read, see the Summary, then consult the Conclusion and Discussion; readers interested in modeling should read Methodology and Mathematical Background before Analysis.

2

Literature Review

2.1. Overview of Vibratory Piling

Vibratory piling is a technique in which piles are installed by applying high-frequency vibrations to reduce soil resistance. The method is widely used in both onshore and offshore projects, with pile types and geometries varying by application—from sheet piles along waterfronts to timber piles near docks. In all cases, the vibratory motion is generated by a VH, the structure of which is described in detail in Section 2.3.

Onshore VH are typically supported by leader systems or suspended from mobile crawler cranes (Fig. 2.1, Fig. 2.2) (International Crane Stakeholder Assembly (ICSA), 2022). Offshore, however, hammers are exclusively suspended from vessel-mounted cranes. This free-hanging configuration is preferred for its extended reach in the marine environment and its compatibility with established offshore lifting practices.

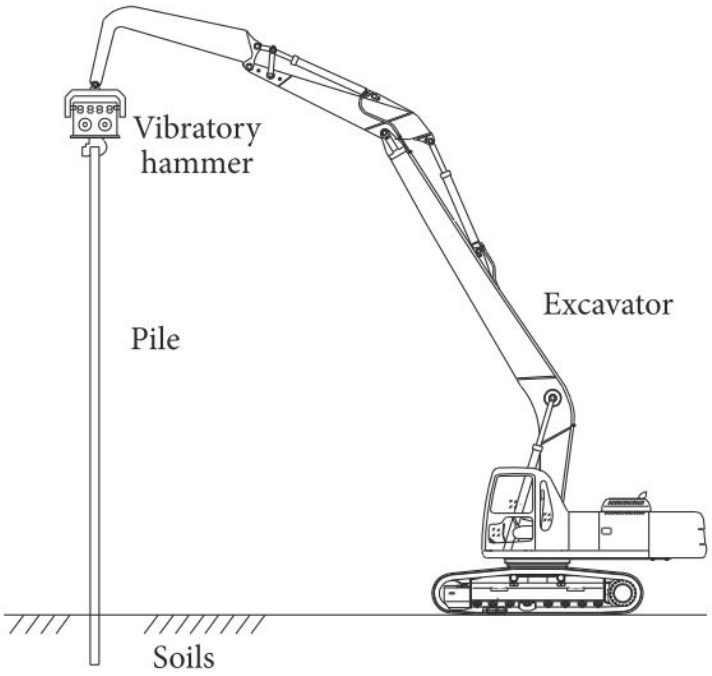

Figure 2.1: Use of excavator as a supporting system, (Viking, 2002)

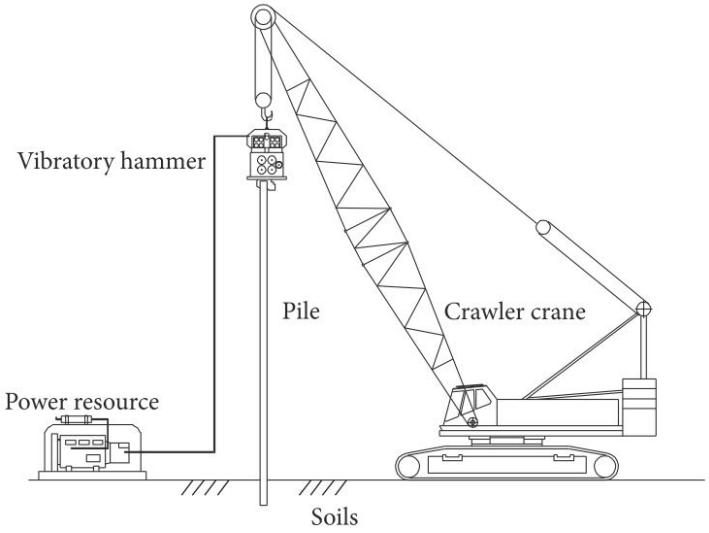

Figure 2.2: Use of crane as a supporting system (Viking, 2002)

Offshore vessels used for vibratory piling fall into two main categories: jack-up vessel (JUV) and floating vessels. JUV are employed in shallow waters up to approximately 50 m depth. Their extendable legs anchor to the seabed and elevate the platform above the waterline, eliminating wave-induced motions and providing a stable base. For deeper waters, floating vessels are used, equipped with dynamic positioning (DP) systems to counteract wave motion during operations.

Deeper offshore installations require monopiles of larger diameter and length to maintain appropriate slenderness ratios. This increase in pile size results in heavier components, which demand higher-capacity cranes and larger installation vessels. Consequently, the scale of vessels, cranes, and piles grows with distance from shore. These scaling requirements have significantly influenced the cost-effectiveness and technical feasibility of fixed-bottom offshore wind farms, and they represent a key factor driving the transition toward floating wind platforms.

Figure 2.3: Use of offshore crane as a supporting system (“Offshore Vibro Piling”, 2023)

2.2. System Components

In general, the components involved in VP can be categorized into three categories:

- Lifting equipment
- Piling equipment

- Environmental

The lifting equipment components are in fact components that are made by Huisman and are point of interest not to be affected by any vibration during the VP operation. Referring to the objectives of study, these components are meant to be investigated. Especially, the lower block with its prong hook as a connecting point to the piling equipment.

Piling equipment contains all the things that their presence means that the operation which is taking place is vibratory piling. For this operation, besides the VH unit with all its individual components mentioned in the Table 2.1, the MP is needed. The connectivity between the Lifting equipment and piling equipment is done via the rigging. Except the MP which is a commonly designed component, piling equipment are designed to not only generate but also stand the vibration, thus, these components are not point of interest for investigation in this study.

Last but definitely not least, components of system is the soil. Soil condition is the most complex and uncertain components of the system because unlike other components, the specification of it is not predetermined and requires field testing which varies location by location and layer by layer in in different depths.

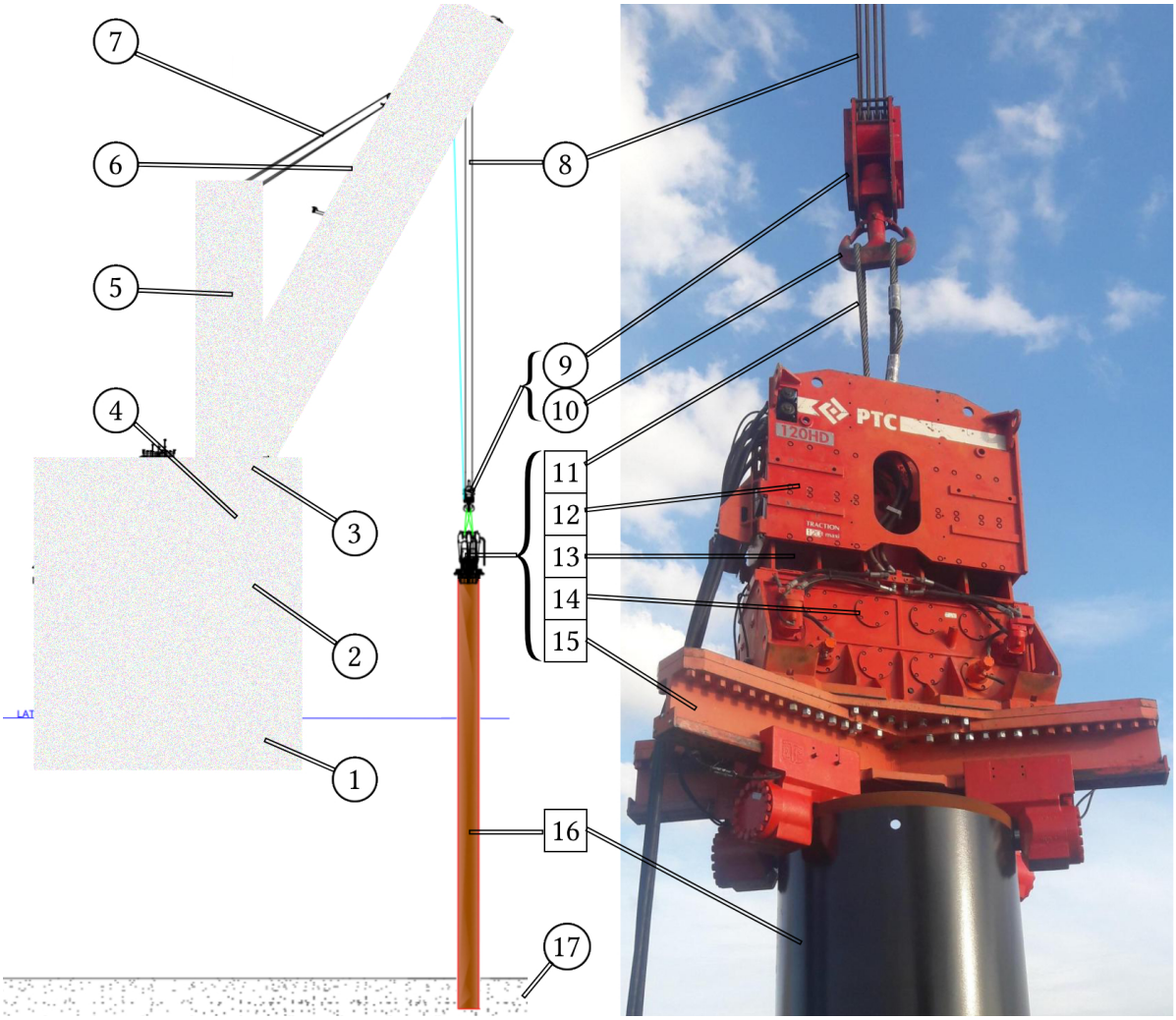

Figure 2.4: system and system components (“Fayat Group VH”, n.d.)

Table 2.1: List of System Components

	Lifting Equipment	Type	Description
1	Vessel	Structure	Base platform
2	Pedestal	Structure	Lower section of crane structure
3	Crane House	Structure	Intermediate section of crane structure
4	Winch Room	Structure	Power room for lifting
5	Luffing Frame/ Mast	Structure	Upper section of crane structure
6	Boom	Structure	Angled section of crane structure
7	Boom Hoist	Wire	Cables pulling the Boom
8	Main Hoist	Wire	Cables pulling payload
9	Lower Block	Structure	Containing sheaves
10	Prong Hook	Structure	Connection/ Crane part
	Piling Equipment		
11	Rigging	Wire	Connection between prong hook and bias mass
12	Bias Mass	Structure	Upper part of VH
13	Elastomers	Connection	Connection between bias mass and exciter block
14	Exciter Block	Structure	Containing sets of eccentric masses
15	Clamping Mechanism	Structure	Rigid connection between Exciter block and MP
16	Monopile	Structure	Steel tube open on both ends
	Environmental		
17	Soil	Environment	Soil conditions requires probe testing

2.3. Vibration Generation

2.3.1. Structure of the Vibratory Hammer

The VH, or vibratory pile driver, is the core equipment in vibratory piling. Its function is to generate cyclic vertical forces that reduce soil resistance and facilitate pile penetration Rainer Massarsch et al., 2022; Warrington, 1992. A typical VH consists of the following components (Fig. 2.5):

- **Suspension Hook**: connection point to the crane hoist line,
- **Bias Mass**: provides a static surcharge force to aid penetration and partially isolates vibrations from the lifting system,
- **Exciter Block**: encases the motors and eccentric rotating masses that generate vibratory forces,
- **Clamping System**: ensures rigid connection between the hammer and the monopile.

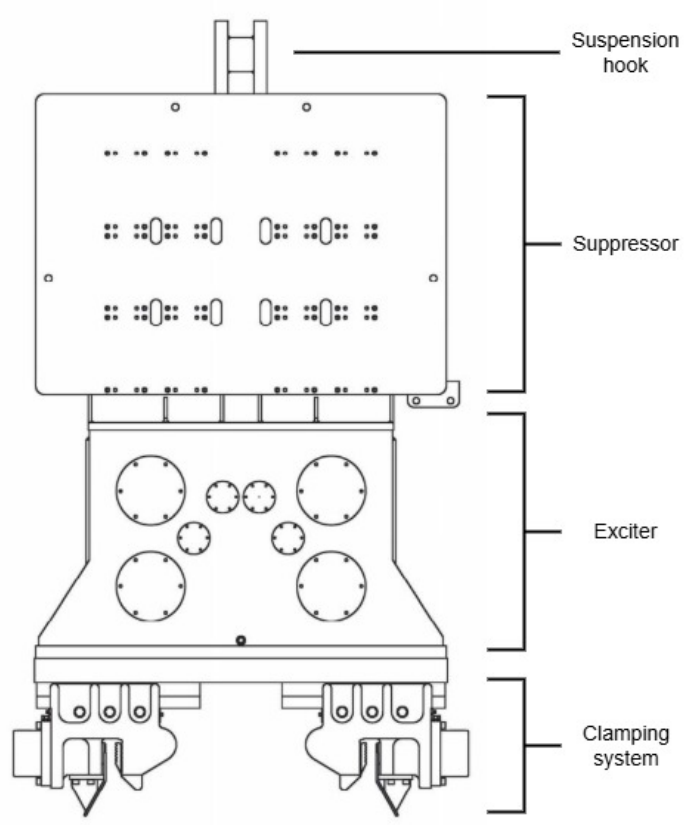

Figure 2.5: Components of a VH unit (“J&M Model 14412T”, 2025)

2.3.2. Working Principle

The VH generates vertical driving forces through counter-rotating eccentric masses. The centrifugal force of each rotating weight is given by:

$$F_c = m_e r_e \omega^2 = M_e \omega^2, \tag{2.1}$$

where m_e is the eccentric mass, r_e its eccentric radius, ω the angular frequency, and M_e the eccentric moment.

By arranging two eccentric masses to rotate in opposite directions, horizontal force components cancel out, leaving a vertical sinusoidal force:

$$F_v = M_e \omega^2 \sin\theta, \tag{2.2}$$

which oscillates at the driving frequency (Fig. 2.6). This cyclic excitation reduces shaft friction and toe resistance, enabling pile penetration with lower energy input compared to impact hammers.

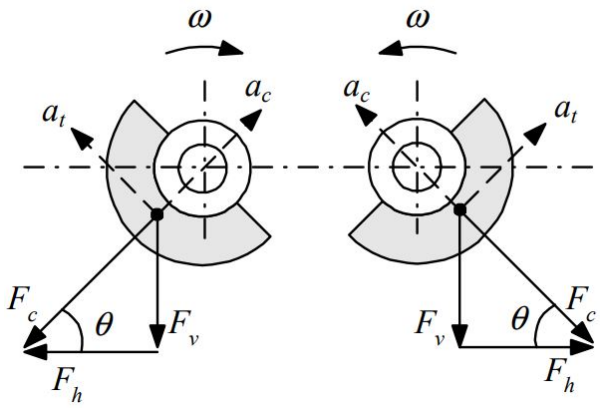

Figure 2.6: Counter-rotating eccentric masses (Viking, 2002)

2.3.3. Vibration Modes

Vibrations generated by the VH can manifest in different modes Rainer Massarsch et al., 2022; Whenham and Holeyman, 2012:

- **Axial Vibration**: the desired mode, producing longitudinal oscillations along the monopile axis to reduce soil resistance and maximize penetration efficiency Tsetas et al., 2023.

- **Radial Vibration**: an undesired mode, occurring due to improper clamping, monopile geometry, or penetration irregularities. It induces lateral deformation of the pile cross-section and reduces efficiency.

Axial vibration is the dominant mechanism in offshore monopile installation, while torsional modes are occasionally applied in soils where shaft resistance is critical Whenham, 2011.

2.3.4. Frequency and Amplitude

The performance of vibratory piling is governed mainly by excitation frequency and displacement amplitude. Recommended ranges for different soil conditions are shown in Fig. 2.7 Rodger and Littlejohn, 1980.

Cohesive soils	Dense cohesionless soils		Loose cohesionless soils	
High acceleration Low displacement amplitude	Low point resistance	High point resistance	Heavy piles	Light piles
Requires high acceleration for either shearing or thixotropic transformation. Predominant side resistance A	High acceleration	Low frequency. Large displacement amplitude		High acceleration
	Predominant side resistance. Requires high acceleration for fluidization A	Predominant end resistance. Requires high displacement amplitude and low frequency for maximum impact to permit elasto–plastic penetration B		Predominant side resistance. Requires high acceleration for fluidization A
Recommended parameters				
$f > 40$ Hz $\ddot{x}$: 6–20 g A: 1–10 mm	f: 10–40 Hz $\ddot{x}$: 5–15 g A: 1–10 mm	f: 4–16 Hz $\ddot{x}$: 3–14 g A: 9–20 mm	f: 10–40 Hz $\ddot{x}$: 5–15 g A: 1–10 mm	

Figure 2.7: Recommended VH parameters for different soils (Rodger and Littlejohn, 1980)

Frequency
The driving force is proportional to the square of frequency:

$$F_v = M_e(2\pi f)^2 \sin\theta, \tag{2.3}$$

indicating that higher frequencies increase vibratory energy Viking, 2002. In practice, soil conditions determine the effective frequency, with field experience showing optimal ranges between 20–40 Hz Feng and Deschamps, 2000; Lee et al., 2012. Efficiency improves when excitation coincides with the natural response range of the pile–soil system, creating resonance effects that enhance penetration Whenham and Holeyman, 2012.

Amplitude
The free amplitude of a VH in air (specified double displacement) is given by:

$$S_{sp} = \frac{2M_e}{m_{dyn}}, \tag{2.4}$$

where m_{dyn} is the vibrating mass. When a pile is attached, the operational amplitude decreases:

$$S_{op} = \frac{2M_e}{m_{dyn} + m_p}, \tag{2.5}$$

with m_p being the pile mass.
Although oscillations are symmetric, penetration occurs due to the presence of a static surcharge (bias) force F_o:

$$F_o = gm_o - T, \tag{2.6}$$

where m_o is the bias mass and T is the crane suspension force. This surcharge shifts the vibration equilibrium downward, producing net penetration per cycle. Experimental evidence confirms that increasing surcharge improves drivability Feng and Deschamps, 2000; Lee et al., 2012.

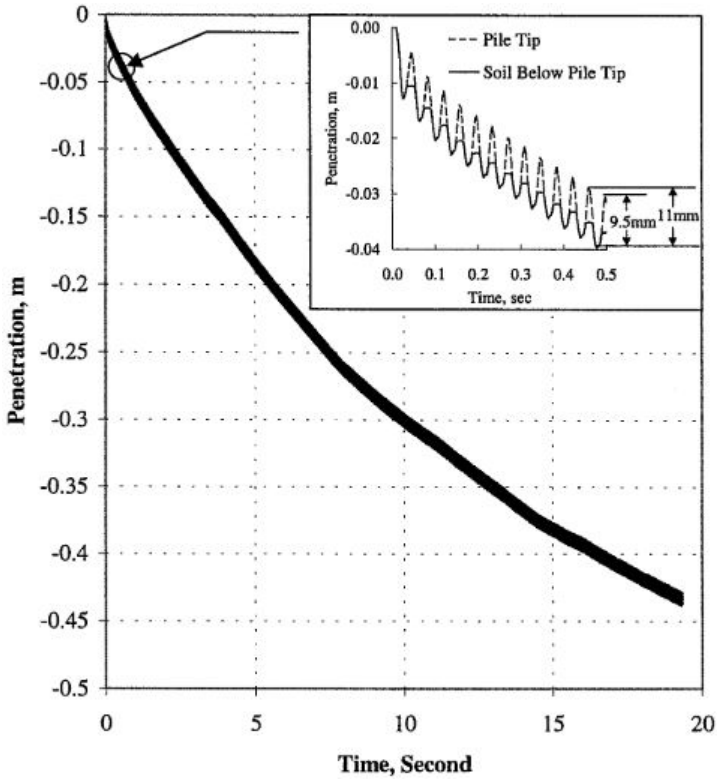

Figure 2.8: Penetration response of a concrete pile under vibratory driving (Feng and Deschamps, 2000)

Modern variable-frequency hammers, such as the CAPE VLT-640, allow operators to adapt excitation frequency during driving, optimizing penetration while limiting excessive vibrations (LLC and Inc., 2024).

2.4. Research Gap

While the effects of vibratory forces on monopile penetration efficiency, soil response, and pile integrity are well-documented, much less attention has been devoted to their influence on offshore cranes. Existing guidelines focus largely on soil–pile interaction and pile–soil damping mechanisms, whereas the risks posed by vibrations to lifting equipment remain largely unaddressed.

The lack of dedicated studies on crane-specific vibratory stress models, fatigue assessments, and vibration isolation techniques leaves a significant blind spot in offshore monopile installation research. Industry recommendations, such as the use of damping systems or constant cable tension, are often based on practical experience rather than systematic experimental validation. Consequently, offshore lifting operations rely on conservative safety margins, which create uncertainty in long-term equipment reliability.

Figures 2.9 and 2.10 illustrate the distribution of reviewed literature, confirming that research to date has emphasized soil and pile behavior while largely overlooking the crane as a critical component.

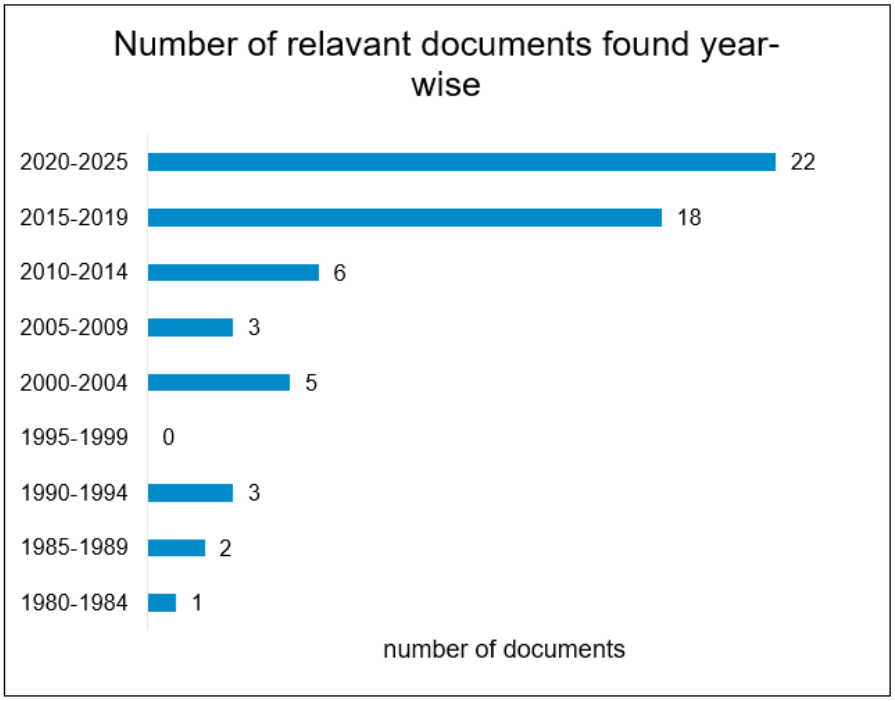

Figure 2.9: Number of reviewed documents sorted year-wise

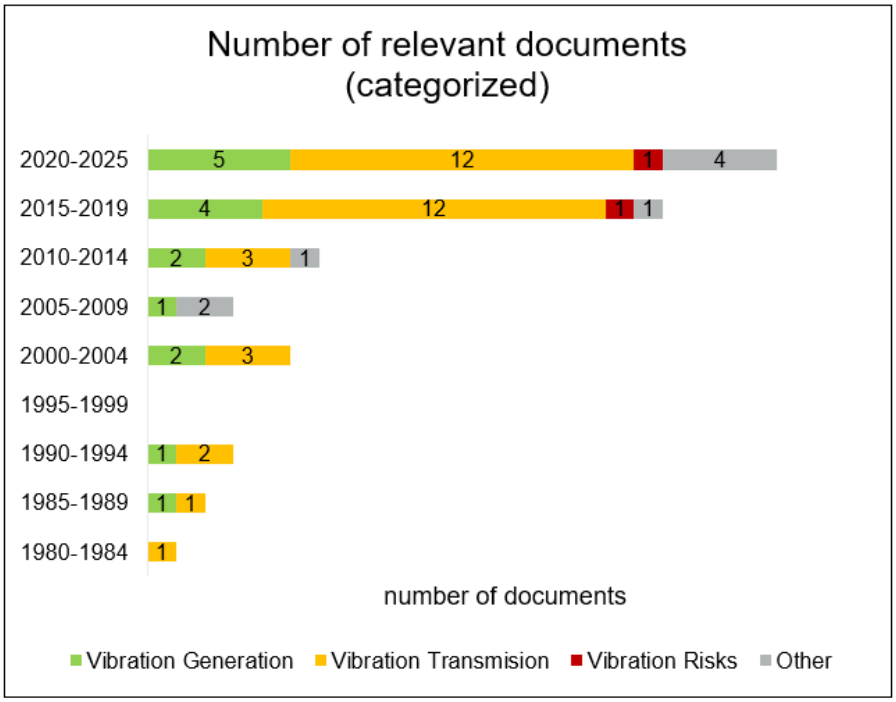

Figure 2.10: Number of reviewed documents categorized and sorted year-wise

Mechanical coupling through the clamping system and residual forces transmitted via tensioned hoist cables allow part of the vibratory energy to propagate into the crane structure. Even when displacements are effectively suppressed, alternating stresses can still reach critical components such as hoist wires and welded joints. Over time, these cyclic stresses may lead to fatigue damage. Such phenomena are not currently accounted for in standard offshore crane design methodologies, leaving operators exposed to long-term degradation risks.

Among all affected components of the installation system, cranes are particularly critical. They combine high financial value with structural complexity and are not easily replaced or repaired offshore. Any degradation or failure can cause significant project delays, financial losses, and safety concerns. Unlike monopiles or hoisting cables, which can be substituted with relative ease, crane components such as the boom or slewing platform are far more difficult to address once damage occurs.
Adding to the challenge is the scarcity of openly available data on crane response to vibratory loading. Monopiles, being relatively simple structures, have been studied extensively through laboratory tests and field monitoring. Cranes, in contrast, are mechanically more complex, integrating structural elements, dynamic cables, hydraulic systems, and real-time load control. Furthermore, proprietary constraints and commercial sensitivities may limit the willingness of manufacturers and operators to publish degradation-related findings.
In summary, this literature review identifies a critical knowledge gap: the vibratory response of offshore cranes during monopile installation. Addressing this gap requires:

1. Developing crane-specific fatigue prediction models that capture continuous high-frequency cyclic loading.
2. Implementing sensor-based health monitoring for early detection of fatigue damage.
3. Investigating advanced vibration isolation systems tailored to offshore lifting equipment.
4. Establishing standardized operational guidelines for de-rating, load limitations, and best practices under vibratory loading.

3

Problem Formulation

3.1. Problem Definition

The problem of vibration transmission arises because the main hoist is not slack during VP; consequently, the entire system remains engaged throughout the operation. This condition causes multiple components to vibrate. From the perspective of the lifting equipment, the lower block, which comprises the prong hook, sheaves, and the frame that accommodates them, together with the hoist cables, remains engaged. Another important component of the crane structure is the boom, which can be affected by vibration. Boom vibration is particularly important because displacement at the boom tip results in vertical displacement of the entire vibratory piling line. To gauge the magnitude of the transmitted vibrations, the most accurate and reliable approach is to set up sensors at various points of the lifting equipment. At the time of writing this thesis, such data are not available. Nevertheless, incident reports indicate that, under certain conditions, the crane operator in the crane house can perceive these vibrations. Because many factors are involved in VP, it is nearly impossible to attribute such incidents to a single cause. Relevant factors include soil conditions at the piling location, piling depth, crane size, MP specifications, VH type, and input frequency. In general, it can be assumed that vibration transmission is most hazardous for crane components at resonance.

3.2. Necessity of Model Development

The extensive literature review revealed that lifting equipment are exposed to vibrations induced by VH. However, the existing studies did not adequately address the level of risk posed to the equipment during onshore vibratory piling, let alone offshore applications, which are a relatively new industry practice. To answer the research question, and in the absence of actual data on the magnitude and frequency of vibrations transmitted to the lifting equipment, such as the crane structure, it is necessary to realistically simulate the vibratory piling environment using available information from previously conducted piling projects. In this way, the system can be examined and the vibrations can be assessed and measured quantitatively.

3.3. Groundwork and Initial Findings

This study will take advantage of available information about VP projects, including reliable data on lifting equipment supplied by Huisman Equipment. Additional information on VH and MP is also available, which ensures that the modeled environment reflects actual VP operations that have taken place. The use of information from a particular case carries the risk of turning a systematic study into a case study; however, this step is unavoidable. It is unavoidable for the same reason explained in Chapter 3.1, namely the numerous influential factors. The risk of becoming a case study can be mitigated by generalizing the system outlook, regardless of crane type, crane size, MP size, or soil conditions.

At later stages, when such generalization risks deviating from realistic conditions, the use of specific assumptions or case-based decisions becomes inevitable, for instance modeling the actual MP.

As mentioned, Huisman has conducted projects related to vibratory piling. However, the limitation of these projects lies in their case-specific nature. A systematic and parameter-generalized approach, as pursued in this study, can provide relief from the time- and cost-intensive evaluation process of cranes.

Notably, the initial findings of Huisman on a specific case serve as a valuable tool for verifying the validity of the generalized approach.

3.4. Objective

The objective of this study is directly linked to the third research sub-question, which concerns the risks posed to the lifting equipment due to vibration. The concept of vibration is related, first, to displacement magnitude and, second, to frequency.
Therefore, the primary objectives of this study are as follows:

1. Measuring the hoist cable force introduced by the presence of VH.
2. Determining the resonance frequency(ies) of the system.
3. Identifying the behavior of each system component with respect to the input frequency of VH.
4. Quantifying the displacement magnitude of each system component.

The first objective reflects the critical concern of VP, namely the role of the hoist cable in transmitting vibration to the crane. The second objective highlights the importance of resonance, which affects all system components. The third objective enables a detailed investigation of the motion of each individual component, with the possibility of later focusing only on those that are part of the lifting equipment. The fourth objective provides a measurable and interpretable quantity of vibration. Together, these four objectives facilitate an understanding of the system and highlight potential risks that may threaten the lifting equipment.
In addition to the above, a secondary objective is defined to ensure that the identified risks for the lifting equipment are evaluated in relation to the piling operation itself.
The secondary objective is as follows:

- Identifying whether the input frequencies that are most effective for pile penetration may also be disruptive or even destructive for the lifting equipment.

This secondary objective ensures that the results of the primary objectives are always cross-checked against the pile penetration procedure.

3.5. Assumptions

The objectives outlined in the previous section require the development of a representative model of the crane and its interaction with the VH. In order to construct such a model and to keep the study both realistic and manageable, a number of assumptions must be defined. These assumptions specify the sources of data, the level of detail to be retained, and the aspects deliberately excluded from consideration. Establishing them at the outset ensures transparency and provides a clear framework for interpreting the results of the analysis.

3.5.1. Sources for Loads and Model

The crane models are implemented based on the design reports of Huisman Equipment. Component masses are taken from the weight overview table provided by Huisman Equipment, which is summarized and shown in Table 6.5. Wire stiffness is obtained from the crane stiffness reports of Huisman Equipment, and the calculation of wire stiffness is explained in Equation 4.25.

Specifications related to VH were shared with Huisman Equipment in previous projects by the supplier of the VH. However, since some of the specifications used in this study, such as the stiffness of elastomers, are classified, the name of the VH manufacturer will not be mentioned and remains confidential.

3.5.2. Exclusion of Stress, Fatigue, and Safety Evaluations

In this study, allowable stresses, allowable fatigue damage, weld safety requirements, and safety factors are not evaluated. These aspects have already been thoroughly assessed during the standard performance evaluation of the crane, which ensures compliance with relevant design codes and safety regulations.

The present research focuses on identifying risks to the lifting equipment arising from vibrations induced during VP. To achieve this, the crane model is generalized and simplified, with emphasis placed on vibration-related parameters such as displacement magnitude, frequency, resonance, and force transmission. Incorporating detailed checks on stresses, fatigue, and weld safety would not be compatible with this generalized approach, as such checks require exact structural details that are beyond the intended scope of this study.
Therefore, the exclusion of these evaluations is deliberate and justified, as the focus of this study is on the vibratory response of the system rather than on its structural design validation. Such evaluations have already been conducted and are documented in the original design reports of Huisman Equipment.

4

Methodology

The aim of this chapter is to construct a model that is representative to a real VP system and simple enough to satisfy all the objectives mentioned in the Chapter 3.4. To achieve such model, some simplifications are required to compensate the complexity of crane models and structures as well as the complexity of environmental uncertainties such as soil conditions. Before any simplification, it is essential to understand the complete system and its components regardless of VH model and crane type.

4.1. Simplification of Crane

The variation in offshore cranes, such as different types and sizes, leads to the challenging question of which crane model should be considered for implementation. To address this, the crane is simplified in two steps. First, it is generalized into a 2D representation. Second, it is converted into an equivalent mass and spring model that can be treated as 1D.

To generalize the cranes, it is first necessary to identify the candidate cranes. By reviewing them and highlighting their similarities, a generalized crane model can then be constructed. The selection of cranes suitable for VP is based on two criteria, either of which qualifies a crane as a candidate:

- the crane has been used in an offshore vibratory piling operation;
- the crane has sufficient capacity to handle piling equipment for XL and XXL MPs.

Based on the available data and catalogs of Huisman Equipment, three crane types are selected: offshore mast crane (OMC), leg encircling crane (LEC), and tub mounted crane (TMC). A common feature among them is that the boom is connected to the crane house at the pedestal, allowing rotation about this point, and the boom angle is adjusted via the boom hoist wires connected to the top of the mast or luffing frame. The main difference between the OMC and the TMC is that the mast in the OMC is stationary and the boom rotates around it using large slew bearings, whereas in the TMC the luffing frame rotates together with the boom. The LEC differs from the TMC in that its pedestal is hollow, allowing the legs of the JUV to move freely within it, facilitated by the wider luffing frame.

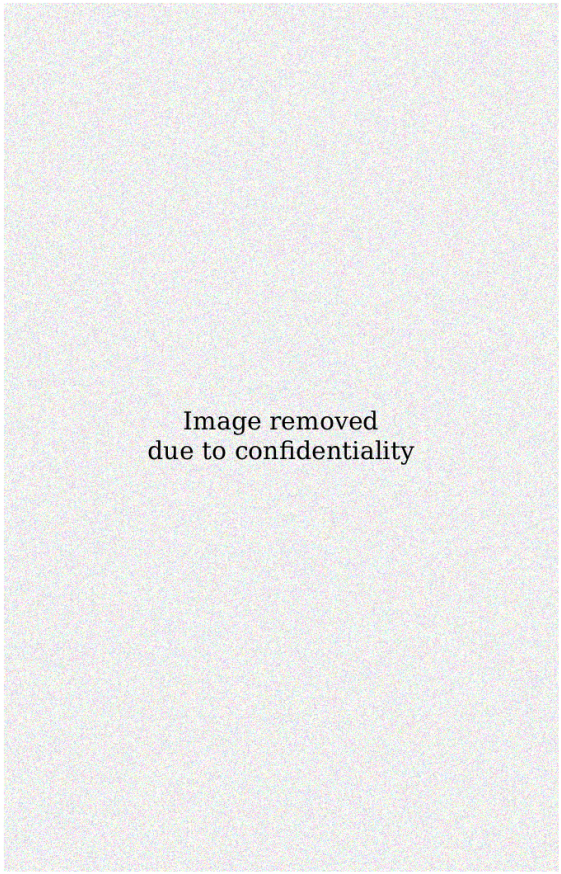

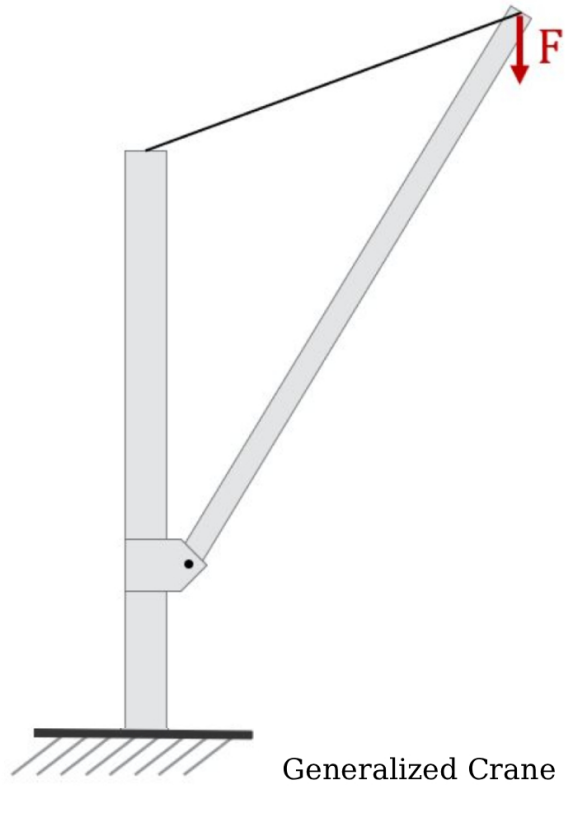

Figure 4.1: (a) On the left: 3 cranes manufactured by Huisman Equipment that are capable of VP at the level of XL and XXL MPs
(b) On the right: The generalized crane

Due to the structural symmetry of these cranes in the Y Z plane, they can be represented in 2D as shown in Fig. 4.1. Although generalized, the actual dimensions such as the height of the mast or luffing frame, the length of the boom hoist, and the boom length remain critical and are retained in the model.

The assumption taken here is that the generalized crane is clamped to a fixed base. In practice, the crane pedestal is welded to the vessel, and the vessel itself is not fixed. This simplification can be justified in two common operating scenarios. First, when the crane is mounted on a JUV, the hull is supported by its legs bearing on the seabed, so the deck that carries the crane behaves as a fixed platform for the time scale of VP. Second, when the crane operates from a floating vessel, DP maintains station and limits low frequency global motions; relative to the higher frequency input from the VH, the residual motions are small, so the pedestal can be idealized as fixed for vibration analysis. If the vessel motions become comparable to the imposed vibrations, this assumption should be revisited.

The generalized crane is then converted into a system of lumped mass and spring. This step enables the entire VP system to be constructed in a linear, one dimensional form. The conversion is admissible because the 2D generalized crane and the 1D equivalent share one degree of freedom (DOF).

To establish equivalence, key characteristics of two models should be matched:

- the kinetic energy of the lumped mass equals the kinetic energy of the generalized crane about the fixed pedestal and mast
- the potential energy in the equivalent spring equals the potential energy stored in the boom hoist.

From these conditions, relationships between the parameters of the generalized crane and those of the

mass and the spring can be derived. Figure 4.2 presents the generalized crane and its 1D equivalent together with the parameters used in the derivation.

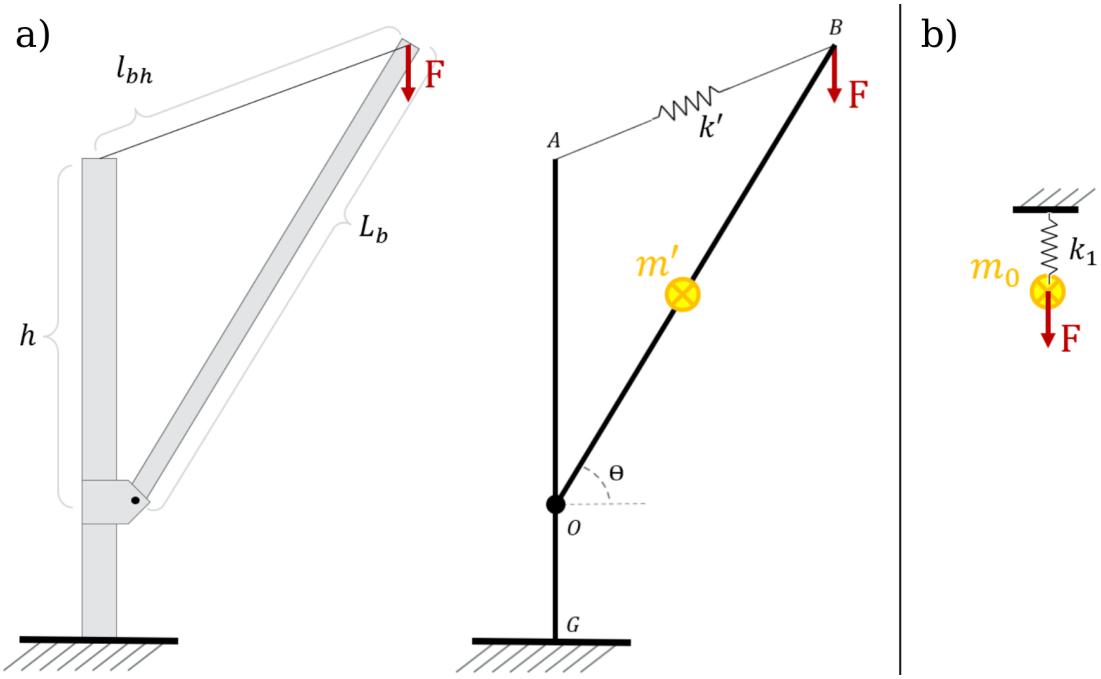

Figure 4.2: (a) On the left: The generalized crane
(b) the equivalent simplified crane with equivalent boom mass and equivalent boom hoist stiffness

Table 4.1: Generalized crane description

Name	Element Type	Description
GO	Rigid and clamped to a fixed base	Pedestal
O	Pivot point	Boom hinge point
OA	Rigid and Clamped to GO	Mast or Luffing frame
OB	Rigid and Pinned to O	Boom
AB	Spring connection	Boom hoist cables

Elements used in of the generalized crane shown in Fig. 4.2 are named and their type are mentioned in Table 4.1.

The only DOF of the generalized crane is rotation of the boom about the pivot point O with angle θ. The only DOF of the equivalent simplified crane is the vertical displacement of the lumped mass along the y axis. To relate the two models, the location of point B (the boom tip) is written as follows:

$$x_b = L_b cos\theta \tag{4.1}$$

where x_b is the horizontal position of point B in a Cartesian plane, L_b is the boom length OB, and θ is the boom angle. Similarly, the vertical position of the boom tip is

$$y_b = -L_b sin\theta \tag{4.2}$$

where y_b is the vertical position of point B in a Cartesian plane.

4.1.1. Equivalent Boom Mass

The lumped mass is called the equivalent boom mass because it represents the boom mass of the generalized crane and is derived by relating the kinetic energies of the two models. Since the pedestal

and mast are assumed fixed, the only kinetic energy is that of the boom rotating about the pivot point O as shown in Fig. 4.2.
The kinetic energy of the boom is

$$T_b = \frac{1}{2} I_b \dot{\theta}^2 \tag{4.3}$$

where T_b is the kinetic energy of the boom, I_b is the moment of inertia of the boom, and $\dot{\theta}$ is the angular velocity of the boom.
The moment of inertia of a boom pinned at one end is

$$I_b = \frac{1}{3} m' L_b^2 \tag{4.4}$$

where m' is the total boom mass. Then the kinetic energy becomes

$$T_b = \frac{1}{2} (\frac{1}{3} m' L_b^2) \dot{\theta}^2 \tag{4.5}$$

Relating θ to y_b, the vertical velocity of the boom tip ($\dot{y_b}$) in terms of $\dot{\theta}$ is

$$\dot{y_b} = \frac{dy_b}{d\theta} \dot{\theta} = -L_b cos\theta \dot{\theta} \tag{4.6}$$

Rearranging gives

$$\dot{\theta} = \frac{-\dot{y_b}}{L_b cos\theta} \tag{4.7}$$

Substituting this angular velocity into the kinetic energy of the boom yields

$$T_b = \frac{1}{6} m' L_b^2 (\frac{\dot{y_b}^2}{L_b^2 cos^2\theta}) \tag{4.8}$$

For the equivalent simplified crane, the kinetic energy of a lumped mass attached to a weightless linear spring is

$$T_m = \frac{1}{2} m_0 \dot{y_m}^2 \tag{4.9}$$

where T_m is the kinetic energy of the lumped mass, m_0 is the lumped mass, and $\dot{y}_m$ is its velocity. Equating the two kinetic energies gives

$$T_b = T_m \tag{4.10}$$

and setting the same tip and lumped mass velocities,

$$\dot{y}_b^2 = \dot{y}_m^2 \tag{4.11}$$

results in

$$m_0 = \frac{m'}{3cos^2\theta} \tag{4.12}$$

This expression shows that the equivalent boom mass m_0 is obtained from the boom mass m' and the boom angle θ.

4.1.2. Equivalent Boom Hoist Stiffness

Similar to the equivalent boom mass, the equivalent boom hoist stiffness is the stiffness of the spring in the equivalent simplified crane representing the boom hoist stiffness.
It is obtained by equating the potential energies of the springs in the two systems and imposing the same displacement for the boom tip and the lumped mass. The potential energy stored in the boom hoist spring of the generalized crane for a small elongation is

$$U_{bh} = \frac{1}{2} k' (\delta l_{bh})^2 \tag{4.13}$$

where U_{bh} is the potential energy in the boom hoist spring, k' is the boom hoist spring stiffness, and δl_{bh} is the small elongation of the boom hoist of length l_{bh}. The boom hoist length is

$$l_{bh} = \sqrt{(L_b cos\theta)^2 + (L_b sin\theta - h)^2} = \sqrt{L_b^2 + h^2 - 2hL_b sin\theta} \tag{4.14}$$

where h is the height of the mast or luffing frame. To find the elongation of l_{bh} with respect to a change in θ, differentiate l_{bh} with respect to θ:

$$\frac{d\ l_{bh}}{d\theta} = \frac{-2hL_b cos\theta}{2\sqrt{L_b^2 + h^2 - 2hL_b sin\theta}} = \frac{-hL_b cos\theta}{l_{bh}} \tag{4.15}$$

The partial derivative of boom hoist length with respect to boom tip displacement is

$$\frac{\partial l_{bh}}{\partial y_b} = \frac{\frac{d\ l_{bh}}{d\theta}}{\frac{dy_b}{d\theta}} = \frac{h}{l_{bh}} \tag{4.16}$$

Rearranging gives

$$\delta l_{bh} = \frac{\partial l_{bh}}{\partial y_b}\delta y_b \tag{4.17}$$

For the equivalent lumped mass and spring model, the potential energy of spring k_1 is

$$U_m = \frac{1}{2}k_1(\delta y_m)^2 \tag{4.18}$$

where U_m is the potential energy in spring k_1, k_1 is the spring stiffness, and y_m is the displacement of the lumped mass that produces the elongation of k_1. Equating the two spring energies,

$$U_{bh} = U_m \tag{4.19}$$

yields

$$k'(\delta l_{bh})^2 = k_1(\delta y_m)^2 \tag{4.20}$$

With the same displacement at the boom tip and the lumped mass,

$$\delta y_b = \delta y_m \tag{4.21}$$

we obtain

$$k_1(\delta y_m)^2 = k'(\frac{-h}{l_{bh}})^2(\delta y_b)^2 \tag{4.22}$$

Therefore, the equivalent boom hoist stiffness in the simplified crane is

$$k_1 = k'(\frac{h}{l_{bh}})^2 \tag{4.23}$$

This shows that the equivalent stiffness depends on the boom hoist stiffness k', the mast or luffing frame height h, and the boom hoist length l_{bh}.

4.2. Simplification of Soil

Interpretation of soil in to the system is the most complex and challenging component to be handled. This complexity stems from the fact that the soil conditions are different from location to location and even in one site, the soil has not the same characteristics within the range of other piling spots. On top of that, soil characteristics are depth dependent meaning that by progression of the pile penetration, the soil behave differently. That is because not only the martial of the sand could be different in other layers of the soil, but also deeper layers are typically denser.
By the increase of depth, the shaft of MP is exposed to the side friction causing stiffness and damping to the monopile. In the literature, there are different interpretation of soil behavior in piling in general.

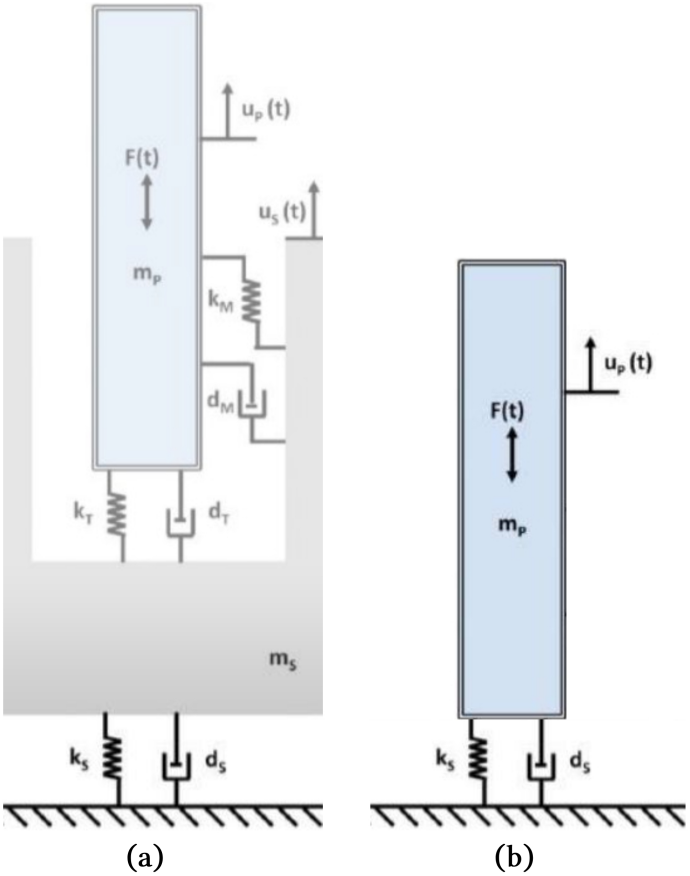

Figure 4.3: (a) Complex model of soil utilized in (Massarsch et al., 2017
(b) Simplification of soil and considering only the stiffness and damping reaction at the toe of MP

One common approach is to assume the soil to be modeled as a pair of spring and dampers. There are other alternatives which are more comprehensive by taking side frictions (aka shaft resistance) into account as shown in Fig. (4.2. However, since the available data for this study is only associated with the toe resistance of the monopile, the effect of shaft resistance is considered with the toe resistance combined and the damping effect as well. The soil stiffness and damping coefficient vary by the change in depth, since the soil characteristics depend on the soil conditions. To discrete the soil characteristics depending on depth, soil conditions are given in different depths. Assuming the maximum pile penetration depth of MP to be 40 meters, the depth pile can be categorized to interval of 5 meters. Meaning there would be 8 different depths, each associated with a different spring damper couple. The influence of depth difference, adds variability to the 3 of the system components, later explained in Chapter 4.3

4.3. Model

Now with the two aforementioned simplifications in Chapter 4.1 and 4.2, the model can be built in a one dimensional linear fashion schematically shown in Fig. [6.9].
The model is comprising of 4 lumped masses (m_0, m_1, m_2, m_3), 5 springs (k_1, k_2, k_3, k_4, k_5), and 2 dampers (c_4, c_5).

Table 4.2 shows every component of the system with its symbol, type (whether it is constant or variable), and a short description.

As mentioned in Table 4.2, k_2, k_5, c_4, and c_5 are variable meaning that they are either depth dependent or frequency dependent.

Hoist stiffness, k_2, is depth dependent because with the progress of piling and pile penetration in to the

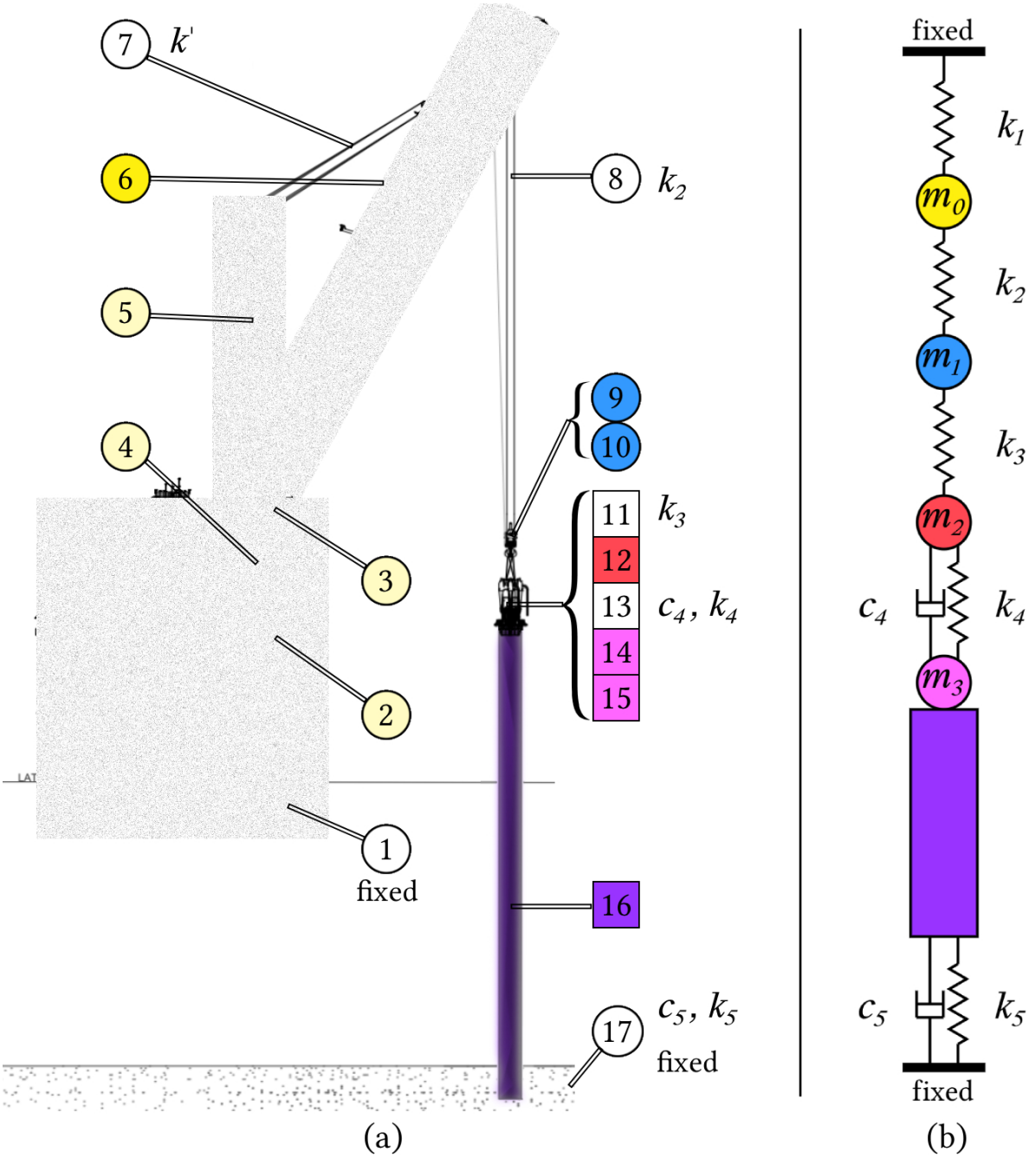

Figure 4.4: Relating the actual system configuration to the simplified 1D system configuration
(a) Color coded actual system configuration and components with the same numbering in Table 2.1
(b) Color coded simplified 1D system configuration

soil, more wire will be fed to the hoist, increasing the length of wire, thus reducing the stiffness of the representative spring.

Soil stiffness, k_5, is also depth dependent. In general, with progress of penetration, the soil resistance increases but the trend of it is not easily predictable and requires field test result from the soil to be determined.

While elastomers stiffness are constant, damping coefficient of them, c_4, is dependent to frequency and is specified by the VH manufacturer. The relationship between the c_4 and input frequency (f_{in}) is as follows:

$$c_4 = a f_{in}^{-b} \tag{4.24}$$

where a and b are numerical factors specified by VH manufacturer.
Similar to soil stiffness, soil damping coefficient, c_5, is depth dependent and in deeper depths, the damping is higher. This coefficient requires field testing of the soil in advance to piling.

Table 4.2: List of Symbols

Mass	Type	Description
m_0	Constant	Equivalent boom mass
m_1	Constant	Lower block mass
m_2	Constant	Bias mass
m_3	Constant	(Exciter + MP) mass
Stiffness		
k_1	Constant	Equivalent boom hoist stiffness
k_2	Variable	Hoist stiffness
k_3	Constant	Rigging stiffness
k_4	Constant	Elastomers stiffness
k_5	Variable	Soil stiffness
Damping		
c_4	Variable	Elastomers damping coefficient
c_5	Variable	Soil damping coefficient

In lifting equipment, the stiffness of wire ropes is calculated as follows:

$$k_{spring} = \frac{n_{falls} \cdot E_{wire} \cdot f_{fill} (\frac{d_{wire}}{2})^2}{l_{spring}} \tag{4.25}$$

where n_{fall} is the number of wire lines in parallel, E_{wire} is the module of elasticity of wire, f_{fill} is the fill factor of the wire, d_{wire} is the diameter of the wire, and l_{spring} is the length of one single line of wire.

4.4. Calculation Method

The calculation method adopted in this study is designed to systematically evaluate the vibratory response of the crane and its interaction with the MP during VP. The scope of the analysis includes the determination of eigenfrequencies, eigenvectors, displacement magnitudes of system components, forces in the hoist wires, and the frequency response function (FRF).

The crane is represented by a simplified model consisting of lumped masses connected by linear springs aligned along a vertical line, as introduced in Section 4.1. The MP is modeled separately as a steel tube using shell elements in finite element analysis (FEA) within Ansys. The springs are assumed to behave linearly, displacements are assumed to remain small, and damping is included only in the forced vibration analysis.

Since the MP itself possesses natural frequencies due to its flexible shell structure, the calculation procedure distinguishes between two steps. First, the MP is assumed to be rigid, so that the resonance frequencies of the crane system can be identified without the influence of monopile flexibility. Second, the MP is considered as a flexible body, and its eigenfrequencies are calculated in Ansys. Among the obtained modes, only the axial flexible-body frequency is retained for the analysis, as it is most relevant to the vertical vibration response associated with VP.

The method then proceeds in two main stages of vibration analysis. In the first stage, a free vibration analysis is conducted to identify the natural characteristics of the system. This involves deriving the equations of motion, formulating them in matrix form, and solving the eigenvalue problem to obtain the eigenfrequencies and eigenvectors. The theoretical background of this step is presented in the Free Vibration section, while the corresponding numerical results are shown in the Modal Analysis

chapter.

In the second stage, a forced vibration analysis is carried out to investigate the system response under harmonic loading. The governing equations are again written in matrix form and solved to determine displacements, wire forces, and the FRF. The theoretical framework of this step is described in the Forced Vibration section, and the corresponding results are presented in the Harmonic Response chapter.

Both stages are solved numerically using Ansys 2022, which provides the computational environment for implementing the equations of motion. In particular, Ansys is employed to transform the system response from the time domain to the frequency domain, which is required for obtaining the FRF.

By structuring the calculation method in this way, the study ensures that the theoretical formulation and the numerical implementation are clearly distinguished. The Free and Forced Vibration sections describe the theoretical basis of the method, while the Modal and Harmonic Response chapters demonstrate its application and the resulting findings.

5

Mathematical Background

5.1. Monopile Structure

The resonance frequencies introduced in the Free Vibration section refer to the dynamic characteristics of the crane system when the monopile (MP) is treated as rigid. However, since the monopile is a steel tubular structure modeled using shell elements in FEA, it also possesses its own natural frequencies associated with structural flexibility. These are referred to in this study as the flexible-body natural frequencies of the monopile.

5.1.1. Monopile Natural Frequencies

As an elastic shell, the monopile can deform in several vibration modes:

- **Axial modes (primary mode in VP):** longitudinal extension and contraction along the pile axis.
- **Bending modes:** lateral deflections of the pile.
- **Circumferential shell modes:** local ovalization ("breathing") of the cross-section.

For a uniform cylindrical pile with length L, density ρ, Young's modulus E, and cross-sectional area A, the fundamental axial natural frequency can be estimated as

$$f_{n_{axial}} = \frac{1}{2L}\sqrt{\frac{E}{\rho}} \tag{5.1}$$

This represents the first longitudinal (axial) mode, while higher-order axial modes occur at integer multiples of this frequency. In practice, a more accurate set of monopile eigenfrequencies and mode shapes is obtained using a shell model in Ansys 2022.

5.1.2. Mode Reduction

Not all monopile modes are relevant for the objectives of this study. Bending, torsional, and circumferential shell modes do not directly couple to the vertical vibration transfer from the crane to the pile. Including them would unnecessarily complicate the analysis. A modal reduction is therefore applied: only the **axial flexible-body natural frequency** of the monopile is retained, as it directly relates to the vertical vibration mechanism of VP.

The analysis is thus performed in two steps. First, the monopile is assumed rigid, and the resonance frequencies f_r of the crane system are determined, as described in the Free Vibration section. Second, the monopile is modeled as flexible, and its axial flexible-body natural frequency is obtained separately from the shell model in Ansys. This frequency is then compared to the crane resonance frequencies to assess potential dynamic interaction.

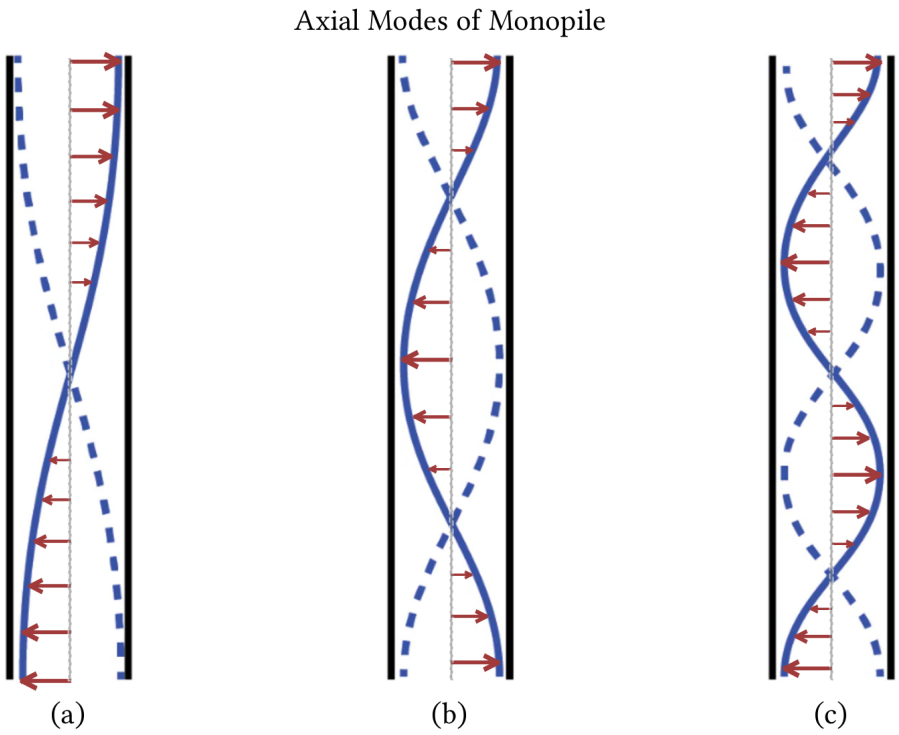

Figure 5.1: First three axial modes of isolated MP with free-free ends. Axial displacements are shown with red arrows on horizontal axis. Dashed lines represent the displacement with 180 degree phase shift.
(a) Fundamental axial flexible body axial mode associated with first flexible-body natural frequency of the MP
(b) Second axial mode of the MP
(c) Third axial mode of the MP

5.2. Free Vibration

The free vibration analysis provides the fundamental dynamic characteristics of the system in the absence of external loading. The equation of motion for an undamped multiple-degree-of-freedom system is expressed as

$$M\ddot{X} + KX = 0 \tag{5.2}$$

where M is the mass matrix, K is the stiffness matrix, and X is the displacement vector defined as

$$X = \begin{bmatrix} x_1 \\ x_2 \\ x_3 \\ x_4 \end{bmatrix}$$

For the generalized crane model, the mass matrix is diagonal and can be written as

$$M = \begin{bmatrix} m_0 & 0 & 0 & 0 \\ 0 & m_1 & 0 & 0 \\ 0 & 0 & m_2 & 0 \\ 0 & 0 & 0 & m_3 \end{bmatrix}$$

The stiffness matrix K is assembled by considering the spring connections between successive masses:

$$K = \begin{bmatrix} k_1 + k_2 & -k_2 & 0 & 0 \\ -k_2 & k_2 + k_3 & -k_3 & 0 \\ 0 & -k_3 & k_3 + k_4 & -k_4 \\ 0 & 0 & -k_4 & k_4 + k_5 \end{bmatrix}$$

Assuming a harmonic solution of the form

$$X(t) = \phi e^{i\omega t} \tag{5.3}$$

where ϕ is the mode shape vector and ω is the circular frequency, substitution into the equation of motion leads to the classical eigenvalue problem

$$\det(K - \omega^2 M) = 0. \tag{5.4}$$

The solutions ω_r obtained from this equation correspond to the resonance frequencies of the crane system when the monopile is assumed rigid. The resonance frequencies expressed in hertz are given by

$$f_r = \frac{\omega_r}{2\pi}. \tag{5.5}$$

The corresponding eigenvectors ϕ_r describe the relative motion of the masses at each resonance frequency.
For consistency and comparability, the mode shapes are mass-normalized according to

$$\phi_r^T M \phi_r = 1. \tag{5.6}$$

This normalization ensures a unique representation of the eigenvectors and facilitates their use in the subsequent forced vibration analysis. It should be noted that in this section f_r denotes the resonance frequencies of the crane system with the monopile considered rigid. The flexible-body natural frequency of the monopile, obtained from a separate shell model in Ansys, will be introduced later in Section 5.1.2.

5.3. Forced Vibration

In contrast to the free vibration case, the forced vibration analysis accounts for the effect of an external harmonic load acting on the system. For the present model, the excitation originates from the vibratory hammer and is applied to the component mass m_3 (representing the exciter and MP). The corresponding force vector is written as

$$F = \begin{bmatrix} 0 \\ 0 \\ 0 \\ F_0 \sin(\omega t) \end{bmatrix}$$

where F_0 is the amplitude of the harmonic excitation and ω is the excitation frequency.
To account for energy dissipation in the system, a damping matrix C is introduced. For the generalized crane model, damping is associated with the elastomers (c_4) and the soil (c_5), and the matrix takes the form

$$C = \begin{bmatrix} 0 & 0 & 0 & 0 \\ 0 & 0 & 0 & 0 \\ 0 & 0 & c_4 & -c_4 \\ 0 & 0 & -c_4 & c_4 + c_5 \end{bmatrix}$$

The governing equation of motion for the damped, forced system can therefore be expressed as

$$M\ddot{X} + C\dot{X} + KX = F(t) \tag{5.7}$$

where X is the displacement vector of the system components, M is the diagonal mass matrix, and K is the stiffness matrix defined in the free vibration section.
Assuming a steady-state harmonic response, the displacement vector can be represented in the frequency domain by its Fourier transform $\hat{X}(\omega)$, which gives

$$(-\omega^2 M + i\omega C + K)\hat{X}(\omega) = \hat{F} \tag{5.8}$$

Here, $\hat{F}$ denotes the Fourier transform of the applied force vector, which corresponds to the complex amplitude of the harmonic excitation. For the present case,

$$\hat{F} = \begin{bmatrix} 0 \\ 0 \\ 0 \\ F_0 \end{bmatrix}$$

The dynamic stiffness matrix is defined as

$$Z(\omega) = K - \omega^2 M + i\omega C \tag{5.9}$$

The harmonic displacement response is then obtained as

$$\hat{X}(\omega) = Z(\omega)^{-1}\hat{F} \tag{5.10}$$

By defining the frequency response function (FRF) matrix as

$$H(\omega) = Z(\omega)^{-1} \tag{5.11}$$

the system response can be expressed compactly as

$$\hat{X}(\omega) = H(\omega)\hat{F} \tag{5.12}$$

This formulation shows that the FRF acts as a transfer function between the harmonic input applied by the vibratory hammer and the displacement response of the crane components. The FRF therefore forms the basis for the harmonic response analysis presented in Chapter 6.2.1, where displacement magnitudes and wire forces are evaluated across the range of excitation frequencies.

6

Analysis

This chapter takes advantage of modeling the system in Ansys and using numerical solution methods. The numerical data used in this chapter were gathered from previous projects carried out by Huisman Equipment.

The analysis is based on a real project that utilized an OMC for a VP operation. The crane used in this project was manufactured by Huisman; therefore, its detailed dimensions and boom mass were available and were used for the crane simplification. Due to the confidentiality of crane exact specifications, the approximated values are giver for mast height and boom mass in Table 6.1.

Data for the lifting equipment are known to Huisman; as the manufacturer, component masses are available for specific cases and can be taken as given. The masses of VP-related components, such as the bias mass and the exciter block, are also known. The stiffness and damping coefficients of the elastomers are available as well. Due to confidentiality, the third party supplier cannot be named and the exact values cannot be cited. These data were provided directly by the respective manufacturers.

The benefit of using actual data is that the risks can be quantified.

The material presented in this chapter directly addresses the research objectives: identifying resonance frequencies, quantifying component displacements, evaluating hoist cable forces, and comparing system dynamics with monopile flexibility.

Crane Specification

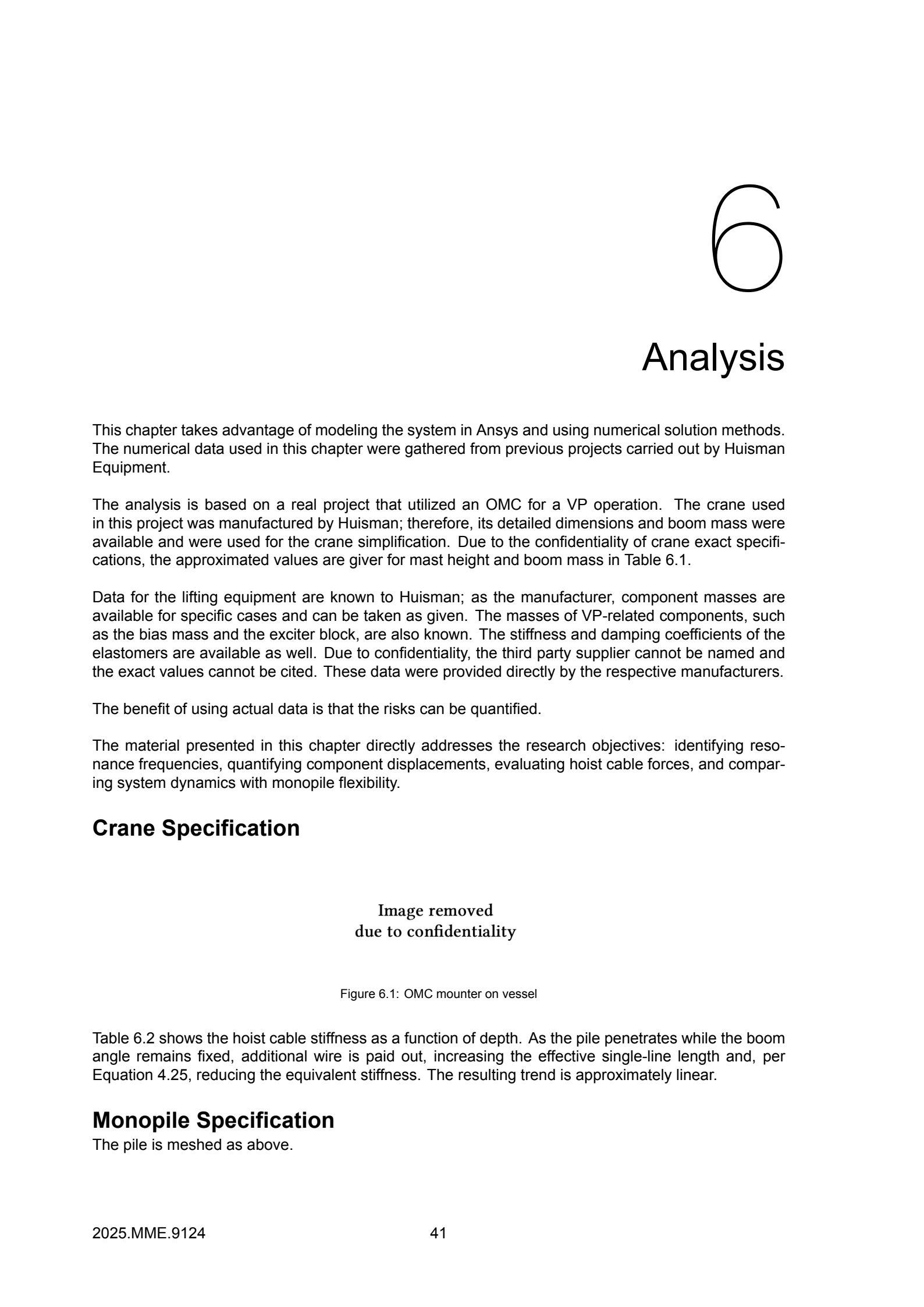

Figure 6.1: OMC mounter on vessel

Table 6.2 shows the hoist cable stiffness as a function of depth. As the pile penetrates while the boom angle remains fixed, additional wire is paid out, increasing the effective single-line length and, per Equation 4.25, reducing the equivalent stiffness. The resulting trend is approximately linear.

Monopile Specification

The pile is meshed as above.

Table 6.1: Crane Specifications (Approximated Values)

Simplified Crane		
Mast Height	h	50-100 m
Boom Length	L_b	75-150 m
Boom Angle	θ	30-80 deg
Boom Mass	m'	
Boom Hoist Stiffness	k'	
Equivalent Components		
Equivalent Boom Mass	m_0	1000-2000 t
Equivalent Boom Hoist Stiffness	k_1	

Table 6.2: Hoist cable stiffness

Depth [m]	**Stiffness (k_2)** [kN/mm]
5	high
10	high
15	high
20	medium
25	medium
30	medium
35	low
40	low

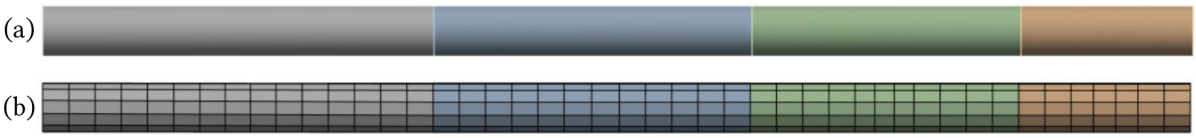

Figure 6.2: (a) Modeled MP in Ansys with 4 sections based on the description mentioned in Table 6.3
(b) Meshed in 45 longitudinal subsections

Table 6.3 shows that the MP used here consists of four sections with the same diameter, while the wall thickness varies by section. In general, lower sections are thicker because bending moments and cyclic stress ranges peak near the mudline during driving and operation, and the soil reaction there increases local buckling demand; increasing thickness reduces these stresses and improves stability under combined loading (Arany et al., 2017; Kallehave et al., 2015).

Vibratory Hammer Specification

Soil Specification

Fig. [6.3] summarizes soil properties at different depths. This depth dependence adds another dimension to the variables and complicates the analysis. The system must be evaluated not only over frequency but also over depth, because k_2, k_5, and c_5 are depth dependent, while c_4 is frequency dependent.

Table 6.3: Pile section dimensions (Approximated Values)

Pile Section	D top [mm]	D bottom [mm]	Wall thickness [mm]	Length [m]
1	4000-5000	4000-5000	75-90	10-20
2	4000-5000	4000-5000	75-90	20-25
3	4000-5000	4000-5000	75-90	25-30
4	4000-5000	4000-5000	75-90	30-35
Total Pile Length [m]				100-120
Total Pile Weight [t]				900-1000

Table 6.4: Vibratory hammer specification

Specification	Value	Unit
Eccentric Moment	1280	kgm
Centrifugal Force	31550	kN
Frequency Range	0-25	Hz
Ramp-up & Ramp-down Range	0-15	Hz
Operational Frequency Range	15-25	Hz

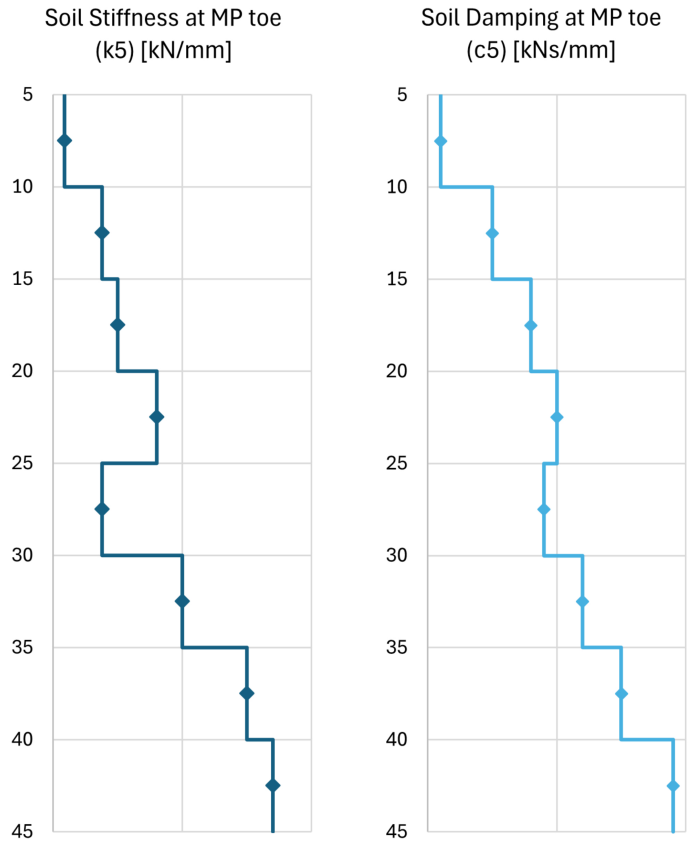

Figure 6.3: An alternative visualization of the soil characteristics change with respect to depth (Approximated Values)

Although soil characteristic data require field testing, it is generally observed that stiffness and damping increase with increasing depth. It is worth noting that there can be situations in which stiffness decreases with depth, as at 25 meters in Fig. [6.3]. This indicates a softer layer at that depth and, if impact hammering were used, could increase the risk of pile run.

Table 6.5 lists the parameters used to represent a specific, close to reality case of VP. All masses are treated as constant. The hoist stiffness (k_2) and soil stiffness (k_5) are depth dependent.

Table 6.5: List of Parameters and Variables of the System (Approximated Values)

Mass	Value	Unit
m_0	2000	t
m_1	100	t
m_2	100	t
m_3	250	t
Stiffness		
k_1	300	kN/mm
k_2	Table [6.2]	kN/mm
k_3	1000	kN/mm
k_4	60	kN/mm
k_5	Fig. [6.3]	kN/mm
Damping		
c_4	Equation 4.24	kNs/mm
c_5	Fig. [6.3]	kNs/mm

6.1. Modal Analysis

Modal analysis is required to determine eigenfrequencies and eigenvectors (mode shapes). Eigenfrequencies identify the frequencies at which the system resonates. Because the system includes an MP that behaves as a flexible body with its own natural frequency, the MP is first analyzed separately to determine its natural frequencies. The resonance frequencies of the combined system are then calculated for two cases, with the pile treated as rigid and as flexible, in order to assess how pile flexibility influences the other resonance frequencies.

6.1.1. Monopile mode reduction

Assuming flexible-body behavior of the MP, the modes are computed and visualized in Ansys. As described in Chapter 5.1.2, the MP exhibits mode families beyond the axial modes. Representative bending and circumferential shell modes are shown in Fig. [6.4] and Fig. [6.5], respectively. These modes appear because the MP is modeled with shell elements.

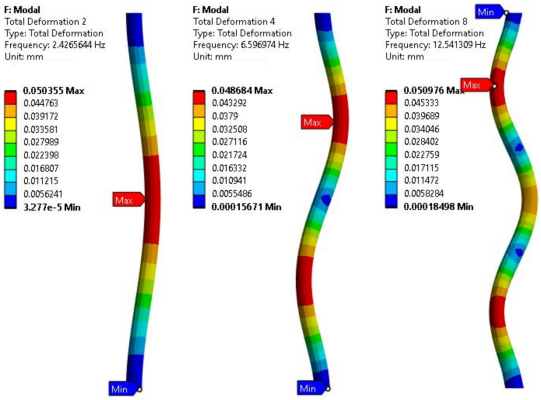

Figure 6.4: Bending modes of the MP

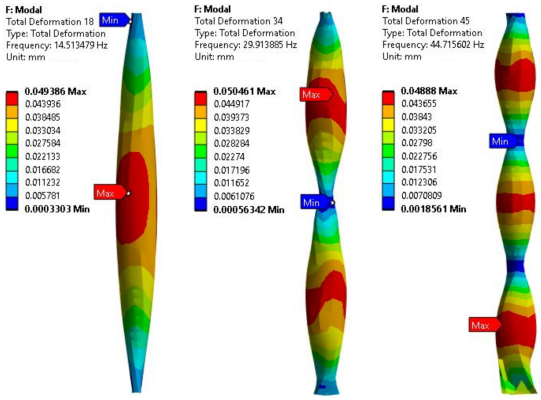

Figure 6.5: Circumferential modes of the MP

Mode reduction is applied because the excitation in VP is predominantly vertical and the adopted model includes only axial coupling. A vertically oscillating driver transmits energy through the pile's axial (vertical) dynamic impedance; under purely vertical harmonic loading, participation of bending or circumferential shell modes is negligible compared with the axial mode family (Gazetas, 1991; Novak, 1977). In the present 1D representation, only axial connections are retained (the elastomer stack k_4 and the soil spring–damper k_5 are axial), so lateral or ovalization modes perform no virtual work on the retained generalized coordinates (modal orthogonality). For completeness, circumferential "ovalization" modes of cylindrical shells exist at higher frequencies but are typically activated by nonuniform radial or lateral loads rather than by uniform axial forcing (Leissa, 1973). If the model were extended to include dis-

tributed lateral soil interaction (e.g., p–y springs) or asymmetric loading, lateral modes would couple to the response and should then be retained (Gazetas and Makris, 1991).

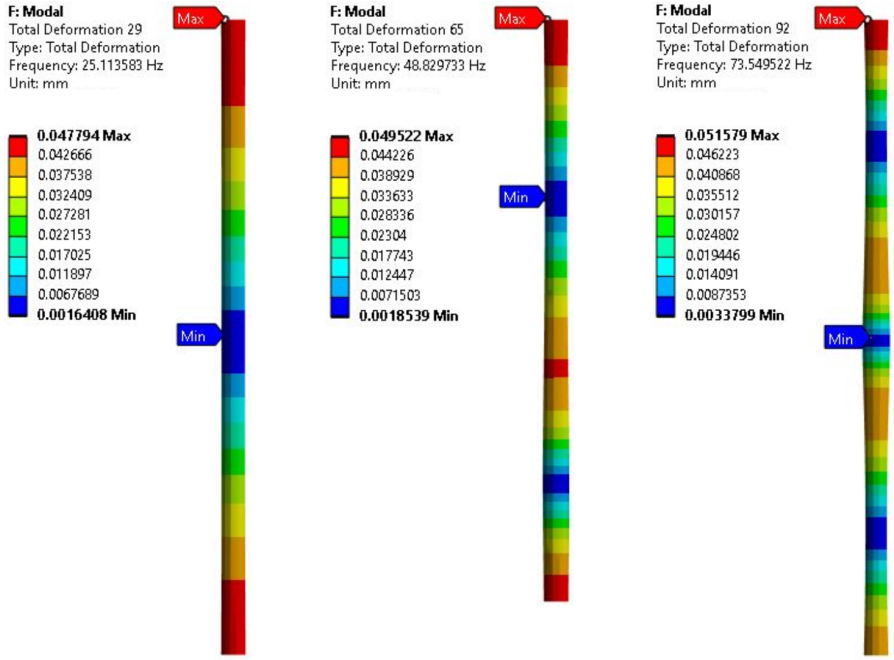

Figure 6.6: Axial Modes of the MP that are most influential on VP

The axial mode of the MP, however, directly affects the behavior of other system components. In the present model the monopile is a free free body, meaning neither end is fixed and axial motion is permitted along the global z axis. In the fundamental axial mode this leads to elongation at both the head and the toe, with the largest axial displacements occurring at the ends. This end elongation activates k_4 at the head through the elastomer connection to the exciter and activates k_5 at the toe through the soil support, which in turn influences the remaining components through the series connection of masses and springs.

Based on Equation 5.1, the axial natural frequency of the isolated MP, made of steel and with a length of 100 m, is calculated as:

$$f_{n_1} = \frac{1}{2L}\sqrt{\frac{E}{\rho}} = \frac{1}{2 \times 100}\sqrt{\frac{2.1 \times 10^{11}}{7850}} = 25.86 \text{ Hz}$$

After the fundamental axial natural frequency of the MP, higher axial frequencies occur at integer multiples of the fundamental (second, third, and so on), as shown below.

$$f_{n_2} = 2f_{n_1} = 2 \times 25.86 = 51.72$$

$$f_{n_3} = 3f_{n_1} = 3 \times 25.86 = 77.58$$

Similar to Chapter 4.3, the model is constructed in Ansys using the variables and parameters listed in Table 6.5. The model is shown in Fig. 6.7. The components correspond exactly to those in Table 4.2. In Ansys, the four discrete masses are positioned on the global z axis and connected in series by axial spring elements k_1 through k_5. Two reference nodes are defined at the system ends to represent the boundaries used for the connections. For the modal analysis, all point masses are constrained in five degrees of freedom and are permitted to translate only in the z direction, which enforces the one dimensional kinematics assumed in the methodology. The monopile is aligned with the same axis and is also restricted to z-directional displacement so that only axial deformation is admitted. No damping elements are included in this chapter, and the eigenvalue problem is solved with the mass matrix and stiffness matrix only.

It is worth noting that the Ansys model allows the MP to be toggled between rigid and flexible behavior under the same boundary and degree of freedom constraints. In the rigid case, the pile is represented by its lumped mass at the exciter location, and k_4 is connected directly to k_5 so that no axial strain develops within the pile while all participating nodes retain only z translation. In the flexible case, the shell representation of the pile is activated with the section properties from Table 6.3; the pile head is connected to k_4 and the pile toe to k_5, and the pile itself remains constrained to z translation only. Using identical constraints in both configurations enables a like for like comparison of eigenfrequencies and mode shapes and isolates the effect of monopile flexibility on the modal characteristics.

Figure 6.7: Modal analysis model

6.1.2. Eigenfrequencies

A modal extraction was performed in Ansys for each penetration depth to identify the resonance frequencies of the system. Two configurations were analyzed: the pile treated as rigid and the pile treated as flexible with only the axial mode family retained after mode reduction explained in Chapter 6.1.1. For consistency, the same boundary conditions and degree of freedom restrictions were applied in both cases, and mode shapes were mass normalized. The results are summarized below as f_{r_i} for system resonance frequencies and f_{n_1} for the monopile axial flexible body frequency. This presentation allows a direct comparison across depths and between the rigid and flexible configurations, and it highlights which frequencies fall within the operational range of the VH.

Table 6.6: List of Eigenfrequencies

Depth	Mode	Rigid	Flexible
20	Mode 1 (f_{r_1})	1.78	1.78
	Mode 2 (f_{r_2})	3.74	3.69
	Mode 3 (f_{r_3})	9.15	7.03
	Mode 4 (f_{r_4})	23.04	23.01
	Mode 5 (f_{n_1})		**23.33**

Table 6.6 lists, for depth 20 m, the system resonance frequencies and the monopile's flexible-body natural frequency.

When the MP is modeled as rigid, its mass is combined with m_3 (the exciter block) because they are assumed to be rigidly connected. This reproduces the formulation in Chapter 5 and yields four system resonance frequencies, which can also be obtained by hand calculation. When the MP is modeled as flexible, the system exhibits four resonance frequencies plus one flexible-body natural frequency after mode reduction.

Comparing the rigid and flexible cases at a given depth shows that Modes 1, 2, and 4 are not appreciably affected by pile flexibility. In these modes the pile remains largely inactive while the lower block and bias mass dominate the response; this is confirmed by the corresponding eigenvectors. In contrast, Mode 3 is sensitive to pile flexibility: pile motion is comparatively large, engaging the soil spring k_5, so depth-dependent changes in k_5 shift this mode.

Focusing on the flexible-pile case and comparing depths individually, the first three resonance frequencies (f_{r_1}, f_{r_2}, f_{r_3}) lie below the lower bound of the VH operational range, while two frequencies (f_{r_4} and the monopile's axial flexible-body frequency f_{n_1}) fall within that range.

A closer inspection of Table 6.6 shows that the two highest frequencies at each depth are separated from the lower modes and are very close to one another, sometimes swapping order with depth. For example, at 15 m penetration, Mode 4 corresponds to f_{n_1} at 22.02 Hz and Mode 5 to f_{r_4} at 23.50 Hz, whereas at 20 m penetration f_{r_4} appears at 23.01 Hz and f_{n_1} at 23.33 Hz. At 20 m, these two frequencies are closer than at any other depth examined; the distinction between them is made by their mode shapes, as shown in Chapter 6.1.3.

6.1.3. Eigenvectors

In addition to eigenfrequencies, the modal analysis provides eigenvectors (mode shapes), as explained in Chapter 5.2. Each eigenfrequency has an associated mode shape that indicates how each component behaves at that frequency. Although every mode influences the entire system, the components are excited to different extents at different eigenfrequencies. The eigenvectors therefore reveal the distribution of motion among components and help distinguish between closely spaced frequencies. To address the discussion in Chapter 6.1.2, all mode shapes for the 20 m depth are visualized.
Fig. 1 illustrates the mode shapes of the system at a penetration depth of 20 meters. These modes correspond to the eigenfrequencies listed in Table 6.6 for the configuration with a flexible MP.

The vertical axis indexes nodes 1 through 50. Nodes 1–4 represent, in order, the equivalent boom mass, the lower block, the bias mass, and the exciter. Nodes 5–50 are the pile centerline nodes created by the mesh discretization. Node 50 is the pile toe, whose displacement is the primary quantity of interest for VP penetration. The pile head shares the same node as the exciter block because they are connected rigidly by assumption.

The horizontal axis shows the globally scaled displacement. At each eigenfrequency, the maximum displacement among all components is scaled to one, and the remaining values are scaled proportionally. This scaling is used because the values arise from a free vibration analysis without external forcing or damping and therefore do not represent physical amplitudes. In the FEA output, eigenvectors are mass normalized and then reported as nodal displacements, so these plotted displacements are equivalent to the eigenvectors defined in Chapter 5.2. Negative values indicate motion in the opposite direction relative to components with positive displacement.

- **Mode Shape 1 (1.78 Hz)**

  At this frequency, the equivalent boom mass has the largest eigenvector, normalized to 1. The lower block and bias mass have positive values of approximately 0.44 and 0.42. The exciter block and the pile nodes are also positive but much smaller (about 0.01 at the exciter and 0.008 at the MP toe), indicating negligible motion for those components. Because all entries are positive, the system moves in phase at this frequency.

- **Mode Shape 2 (3.69 Hz)**

  The boom mass has an eigenvector of about -0.04, while the lower block and bias mass are approximately 1.00 and 0.99. The exciter through the pile show small positive values (about 0.05 to 0.03). The negative sign for the boom indicates motion opposite to the other components. The near-equality of the lower block and bias mass values indicates that these two move essentially together.

- **Mode Shape 3 (7.03 Hz)**

  The exciter block is dominant with an eigenvector of 1.00, and the pile toe is about 0.68. The boom mass is nearly stationary (about 0.006), while the lower block and bias mass are -0.46 and -0.42. The opposite signs again indicate counter-phase motion between the upper masses and the exciter–pile assembly.

- **Mode Shape 4 (23.01 Hz)**

  Most components are close to zero except the lower block and bias mass, which are about 1 and -0.85. Although this frequency lies within the operational range of the VH, the pile contribution is negligible; the response is concentrated in the lower block and bias mass.

- **Mode Shape 5 (23.33 Hz)**

  This corresponds to the MP axial flexible-body natural frequency. The exciter and MP head are about -0.93, the mid-height node (e.g., node 23) is near zero (about 0.009), and the MP toe is about 0.98. The opposite signs at head and toe with a near-zero middle confirm the fundamental axial mode shape (elongation at both ends). Other components are also affected: the lower block and bias mass are approximately -0.30 and 0.28, while the boom mass remains effectively stationary (about 0.0008).

- **Mode Shape 6 (44.94 Hz)**

  This frequency lies above the operational range of the VH and is included for validation. It represents the second axial flexible-body mode of the MP. Two internal near-zero nodes are observed (e.g., nodes 12 and 37 with values about 0.05 and 0.04), consistent with the expected shape for

the second axial mode and its approximate doubling relative to the fundamental, as discussed in Chapter 5.1.2.

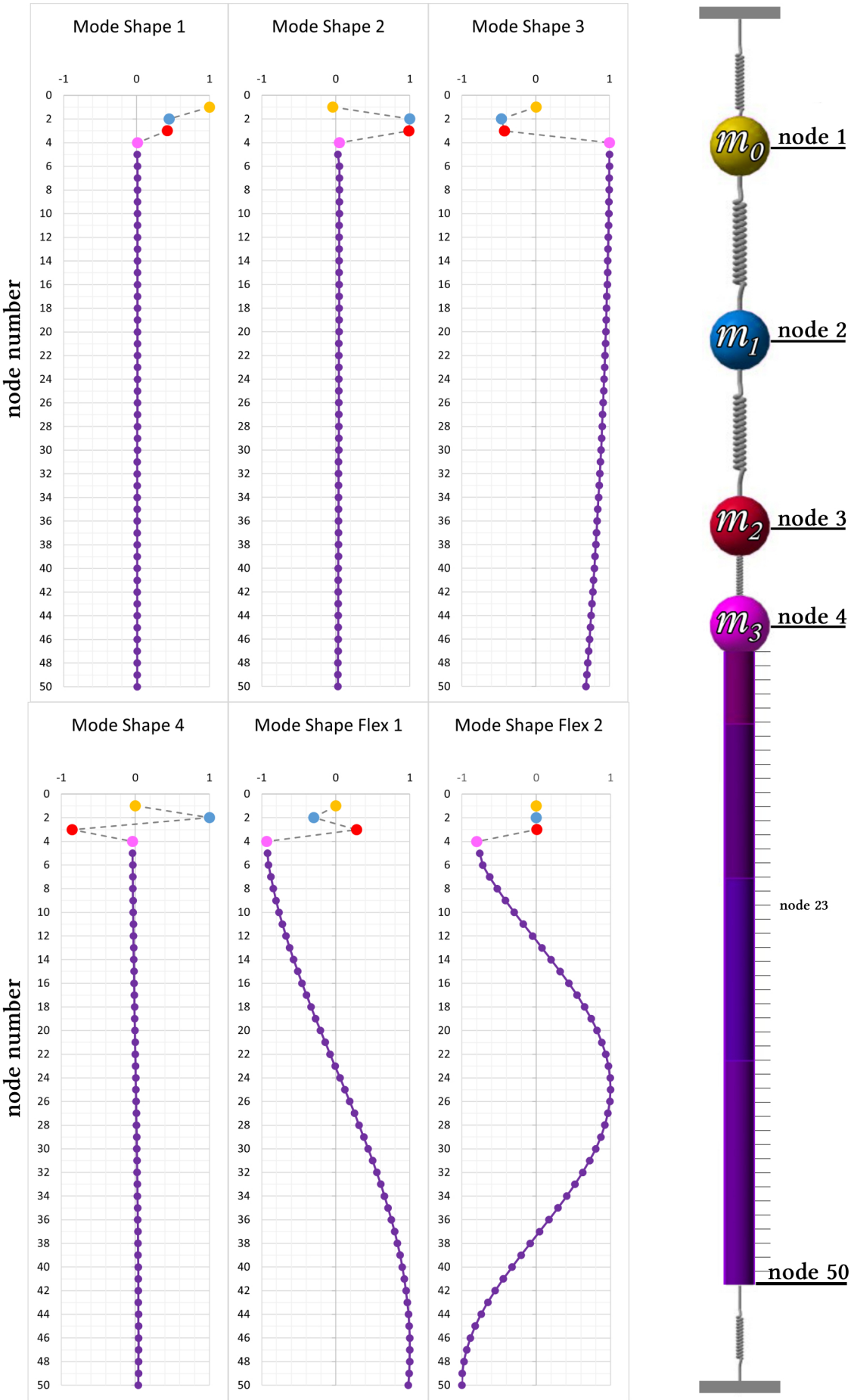

Figure 6.8: Mode Shapes of system with flexible monopile at depth 20 meters.

6.2. Harmonic Response Analysis

In the harmonic response analysis, as outlined in Chapter 5.3, both the external force and damping are included. Fig. 6.9 shows the system with c_4, c_5, and the harmonic input F_0. As listed in Table 6.5, none of these quantities is constant: k_2, k_5, and c_5 vary with depth, while c_4 and the force amplitude generated by the exciter depend on frequency. Unlike the modal results, the harmonic solution yields physical displacement amplitudes, so additional scaling is not required. As a result, when the input frequency coincides with an eigenfrequency, peak displacements are expected.

Because several parameters depend on depth or frequency, the response must be evaluated over both dimensions. Depth dependence requires rebuilding the model at each depth to update k_2, k_5, and c_5, while frequency dependence is addressed by sweeping the excitation frequency.

The FEA environment enables efficient frequency sweeps for a chosen depth. Depth dependent parameters, however, must be updated explicitly, which results in eight models for the eight penetration levels. For consistency with Chapter 6.1.3, the detailed results presented here focus on the 20 m case. Other depths were also analyzed and exhibit similar trend..

Finally, the close connection to the modal analysis is evident in the harmonic results. The resonance frequencies identified in the modal extraction govern the peaks in the frequency response, and the associated mode shapes are reflected in how the displacement is distributed among components at those peaks.

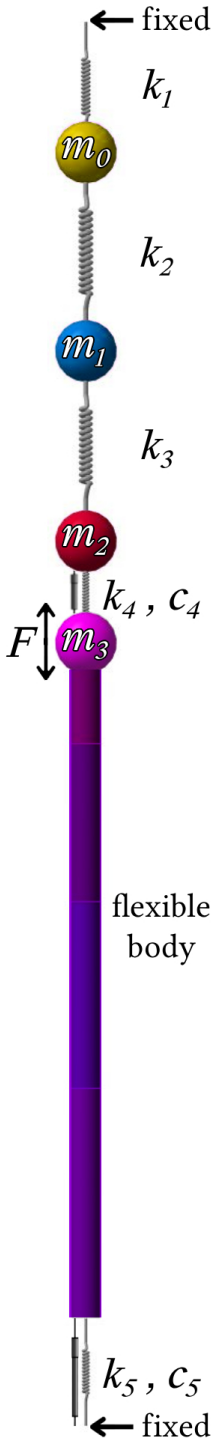

Figure 6.9: Harmonic response analysis model

6.2.1. Frequency Response Function (FRF)

The benefit of using finite element method (FEM) is clear for computing the frequency response. The frequency response function (FRF) maps a harmonic input to the steady-state output entirely in the frequency domain. As described in Chapter 5.3, the complex displacement for each component is obtained from Equation 5.12. Its magnitude, taken directly from the frequency-domain solution, is the steady-state displacement amplitude at that input frequency. This provides the maximum steady-state response without time marching and without sensitivity to transient decay or the chosen simulation window.

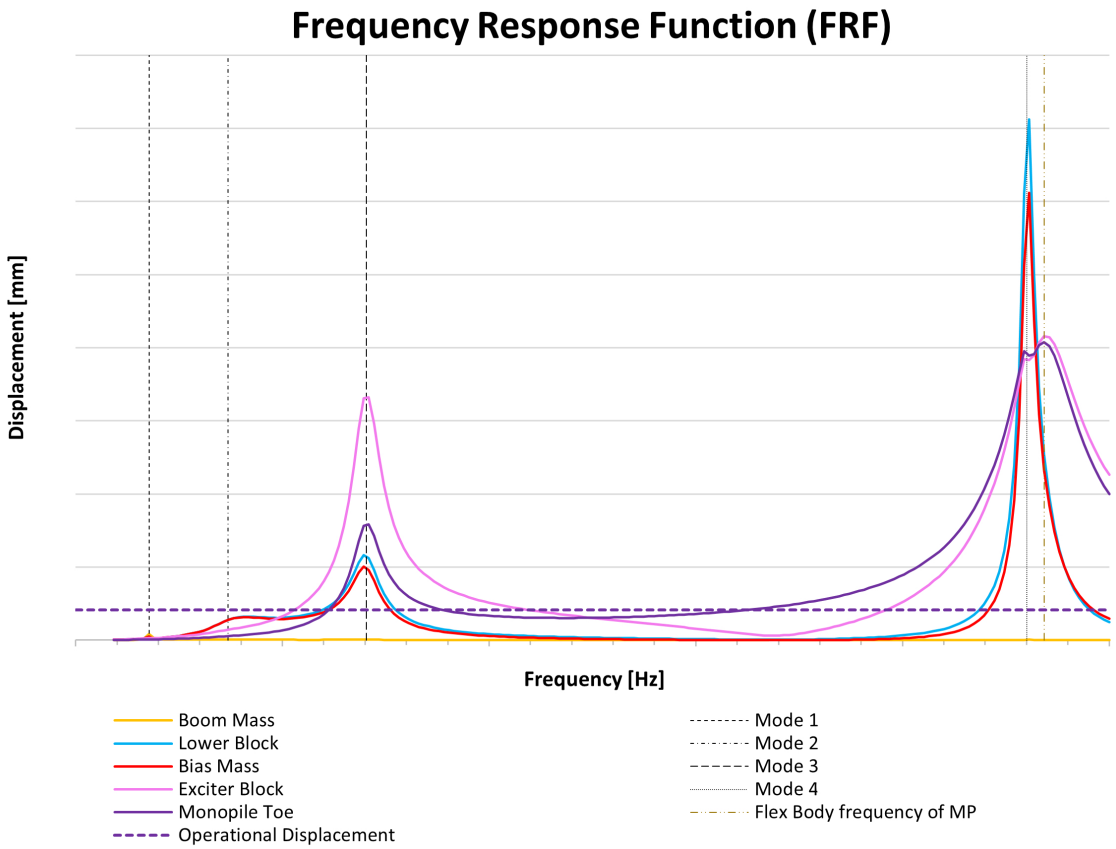

Figure 6.10: Absolute maximum displacement of all the components in frequency domain.

Fig. 6.10 shows the absolute displacement of each system component versus frequency up to 25 Hz, the upper bound of the VH operational range. The vertical guide lines indicate the modes identified in the modal analysis, so peaks in displacement occur at the system eigenfrequencies, as expected. For the 20 m case, Table 6.6 lists five eigenfrequencies at 1.78 Hz, 3.69 Hz, 7.03 Hz, 23.01 Hz, and 23.33 Hz; these are marked on the plot as dashed lines.

- **Frequency 1.78 Hz**

  All components have small displacements on the order of less than a millimeter. The equivalent boom mass is largest. The lower block and bias mass have roughly equal displacements, while the exciter block and pile toe are less than 0.1 mm. The relative magnitudes are consistent with the patterns seen in Chapter 6.1.3, where scaled eigenvectors indicated similar component participation.

- **Frequency 3.69 Hz**

The boom mass, lower block, bias mass, exciter block, and pile toe have displacements of mm, mm, mm, mm, and mm, respectively. The peak response is mainly in the lower block and bias mass, while the remaining components show limited amplification, consistent with the mode shape in Fig. 1.

- **Frequency 7.03 Hz**

  The first pronounced peaks occur at this frequency. The pile response is dominant: the head (at the exciter connection) is mm and the toe is mm, indicating elastic elongation of about mm. The boom mass is nearly stationary at mm; the lower block and bias mass are mm and mm.

- **Frequency 23.01 Hz**

  The response is concentrated in the lower block and bias mass, peaking at mm and mm, which are the largest displacements on the plot. The boom mass is mm; the exciter block and pile toe are mm and mm.

- **Frequency 23.33 Hz**

  The pile exhibits the largest deformation among all components. The head (at the exciter connection) is mm and the toe is mm; from the mode shapes, these occur in opposite directions, implying a maximum axial elongation of roughly mm during VP.

To provide a baseline for the minimum displacement of a pile attached to the exciter outside the full system configuration, a rule of thumb from (Viking, 2002) is used:

$$S_{op} = \frac{2M_e}{m_{dyn}} = \frac{2M_e}{m_{eb} + m_{cl} + m_p} = \qquad mm \tag{6.1}$$

That being said, the target displacement at each depth depends on the local soil properties, specifically the displacement amplitude and the frequency at which the soil exhibits its most favorable temporarily fluidized response.

6.3. Verification

Now that the displacement of each component has been obtained, it is necessary to check whether the system with the adopted crane and soil simplifications is representative of a real life configuration.

The most reliable approach would be to design a test setup and measure responses on the actual components. Strain gauges could be installed at the head and the toe of the MP so that measured strains can be related to the nodal displacements discussed in Chapter 6.2.1. Additional sensors could be placed on other components, such as the lower block, to verify their displacements at selected depths and input frequencies. Any field measurements would need appropriate filtering to remove disturbances caused by environmental conditions such as wind and waves.

At the time of writing, such measurements are not available. What is available is a full FE model that includes a detailed crane representation as shown in Fig. [6.11. This detailed model uses the same soil simplification. By comparing the responses of the detailed full FE model with those of the simplified 1D system, the suitability of the crane simplification can be assessed and the results of the present analysis can be corroborated.

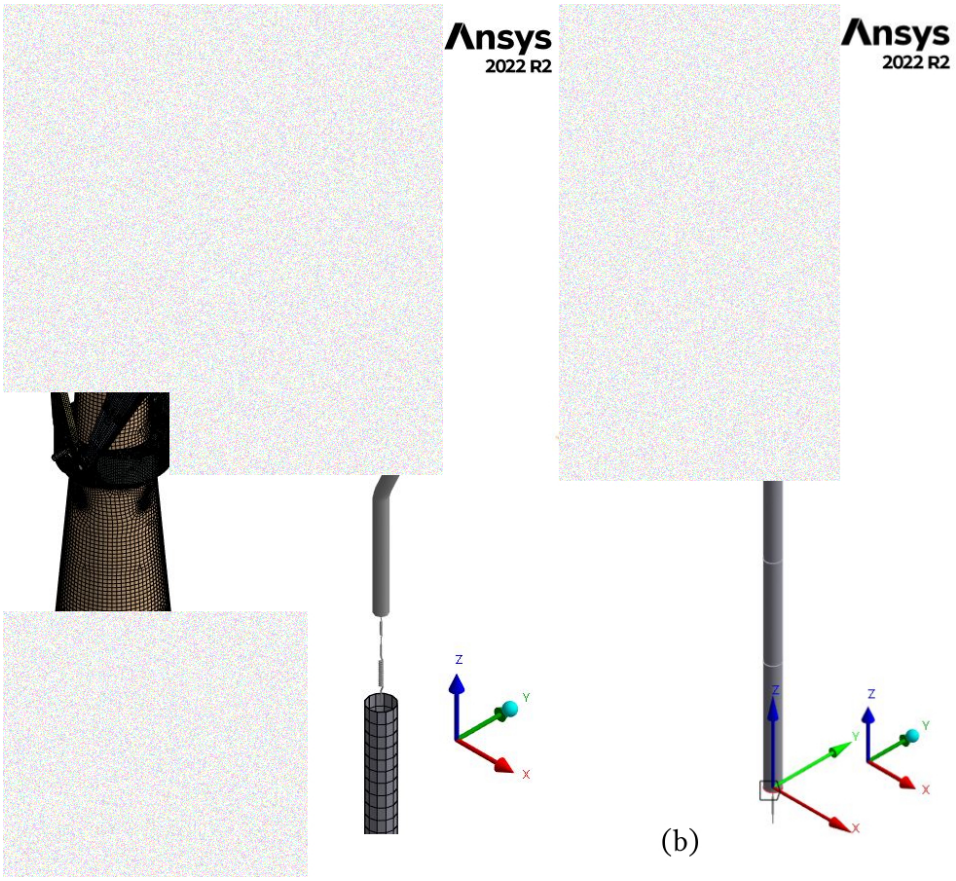

Figure 6.11: Full FE model of the crane, replaced instead of the equivalent boom mass and equivalent boom hoist stiffness.
(a) Meshed model of OMC.
(b) FE model of OMC with additional point masses on crane structure.

There are two criteria for comparing the simplified crane with the full FE crane model. The first is the boom tip displacement, which reflects how the global crane structure responds to vibratory excitation. The second is the hoist cable force, which reflects how the excitation is transmitted through the lifting line into the crane. Together, these two quantities indicate whether the simplified representation preserves both the kinematic response and the load path of the detailed model over the relevant frequency range.

6.3.1. Boom Tip Displacement

Comparing the boom tip displacement from the system with the simplified crane to the displacement from the detailed crane model reveals differences and any peaks that may be missed due to the assumptions in Chapter 4.1. For both models, the same boundary conditions, penetration depth, and excitation range are used, and the same frequency resolution is applied in the sweep so that peak locations can be compared one to one.

As shown in Fig. 6.12, the yellow curve is the boom tip displacement at depth of 20 m for the simplified model, while the gray curve is the corresponding boom tip displacement from the detailed full FE crane model at the same depth. The first peak of the 1D system matches the first peak in the detailed model, which indicates that the simplified representation captures the dominant global mode that governs low frequency response. Additional peaks appear in the detailed model, some of which exceed the first peak and fall within the operational frequency range of the VH. These peaks are not present in the simplified model because they arise from local structural flexibility of the boom and mast that is not represented in the one dimensional chain.

Since the only difference between the two models is the crane representation and the remaining parts of the system are identical, the larger boom tip displacements in the detailed model can be attributed to the flexibility and local modes of the boom and mast. The substructure of the mast, boom and boom

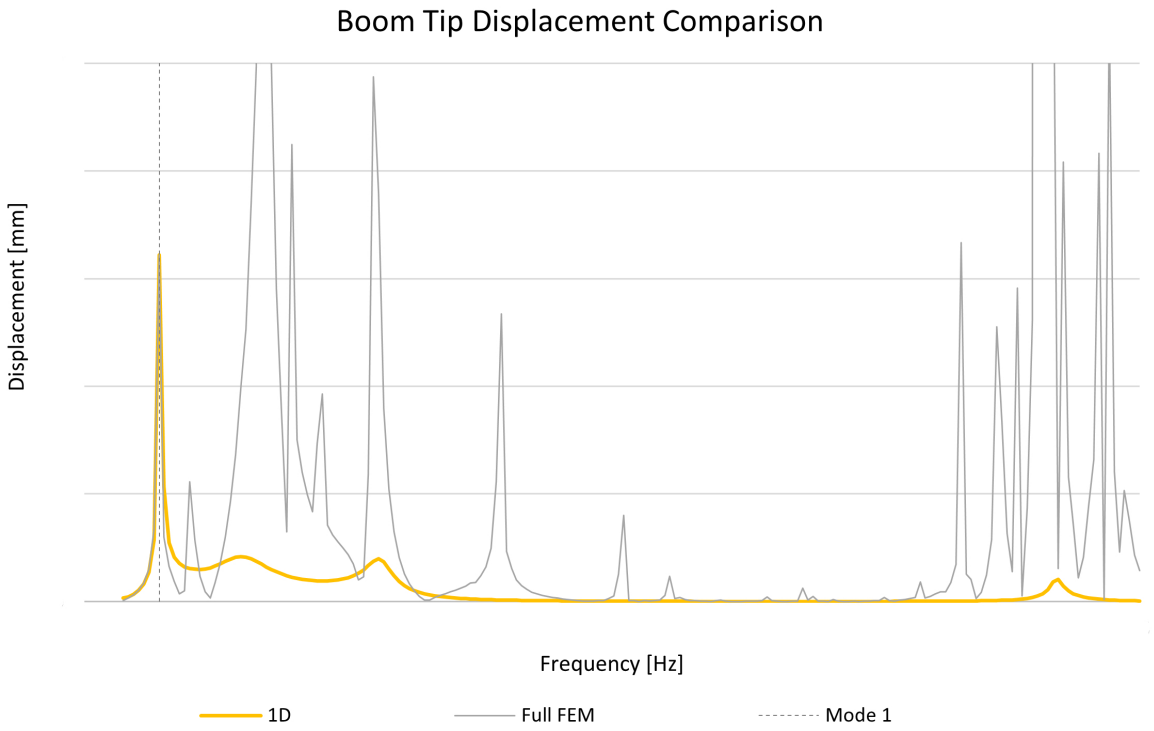

Figure 6.12: Comparison of absolute maximum boom tip displacement between the Full FEM and simplified 1D system.

tip (jib) is shown in Fig. [6.13]. Increasing the stiffness of those substructures so that they behave closer to a rigid body would be expected to reduce these peaks in the detailed model and bring the two responses closer together.

Figure 6.13: (a) Detailed crane house mounted on the mast.
(b) Detailed boom structure.
(c) Detailed boom tip.

Differences are especially evident between 20 Hz and 25 Hz. In this band the lower block exhibits large displacement amplitudes, as shown in Chapter 6.2.1. That motion increases the fluctuation of force transmitted into the boom, which activates higher frequency crane modes in the detailed model. To determine whether the force transmission explains the observed differences, the hoist cable force is compared between the two models in the next subsection.

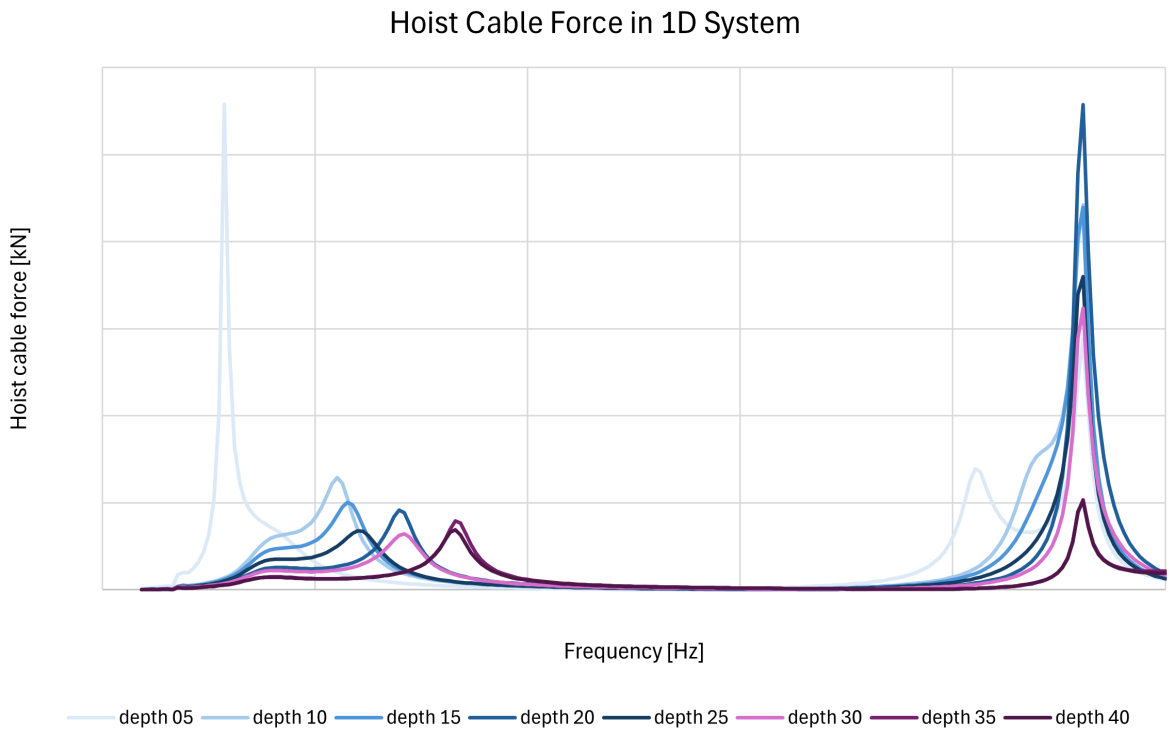

Figure 6.14: Hoist cable force in simplified 1D system for all different penetration depths

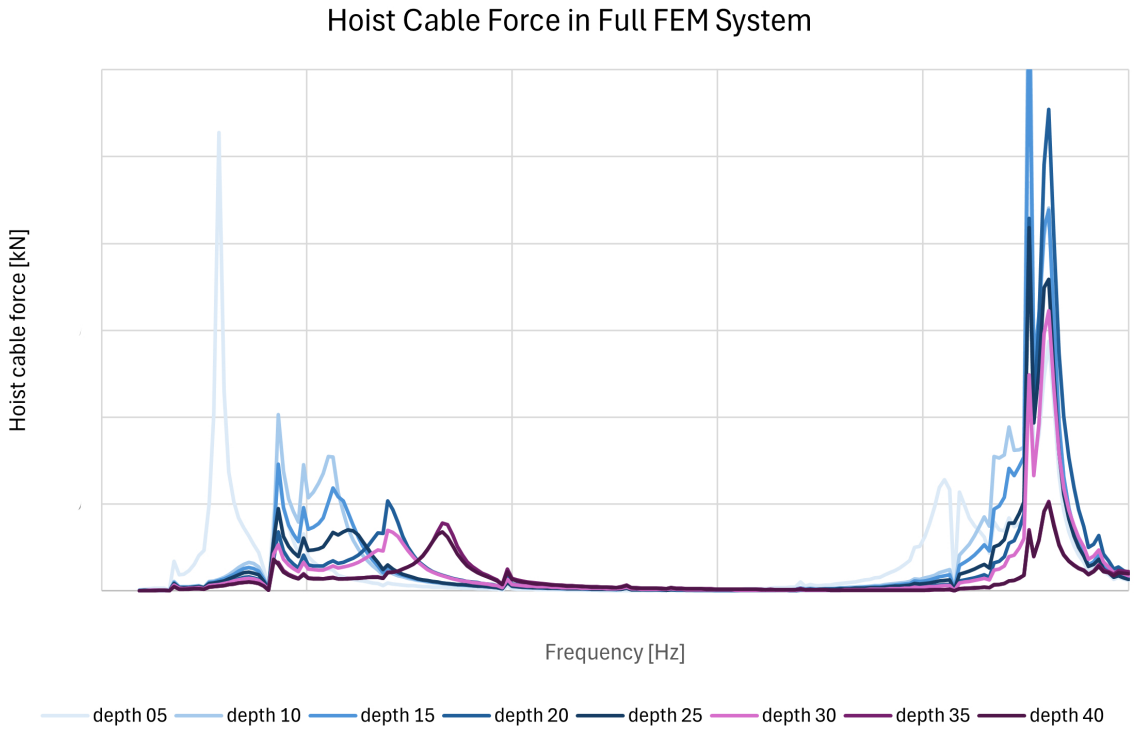

Figure 6.15: Hoist cable force in full FEM system for all different penetration depths

6.3.2. Hoist Cable Force

Comparing Fig. 6.14 with Fig. 6.15 shows broad agreement in hoist cable force across depths, with notable differences at specific frequencies. Since all non-crane components are identical between

models, the deviations arise from the boom and mast substructures in the full FE model (geometry and bending stiffness). On closer inspection, distinct peaks near 4 Hz and 22 Hz appear in the full FE results but are absent in the 1D model; the remaining amplitudes are similar. These peaks are consistent with flexible crane modes that the 1D representation does not include. Intervals of near-zero hoist force likely correspond to in-phase motion of the lower block and boom tip, minimizing line stretch, whereas the large peak near 4 Hz suggests out-of-phase motion that maximizes line extension and tension. The feature near 22 Hz points to a higher crane mode activated by the same coupling mechanism. These interpretations warrant further verification by extracting the relevant crane eigenmodes from the detailed model and examining phase relationships (e.g., operational deflection shapes) to identify which eigenfrequencies govern the observed force peaks.

7

Proposed Solution

This chapter aims to address what could solve the issue of still existing boom tip displacements in the Full FE model. It was mentioned in Chapter 6.3 that the observed vibration in full FEM and not observed in the 1D system with simplified crane is due to the structure of the boom in detailed model of the crane. The reason that crane structure is engaged is due to the force applied to the crane via the hoist cable. Transferred force can actually trigger the flexible body natural frequencies of crane structural elements and results in the displacement of the tip of the boom while it has been assumed to be rigid in crane simplification process.

By the elimination of that force, it is expected that the observed differences are gone and the boom tip displacement the same in both 1D and detailed (full FEM) systems.

The solution for eliminating the cable force can be two options, one is the hard option and the other one is the soft option and they are as follows:

1. disconnecting the hoist cable from the piling equipments
2. implementing an isolator

The first option as the hard and strict option brings us back to where we started as the problem definition to where it was explained why the hoist cable is constantly attached to the piling equipment. Disconnecting the hoist cable guaranties that the crane structure is not engaged during the VP operation thus no cable force nor boom tip displacement will be observed. This approach changes the entire model built in Chapter 4.3. Although favorable from lifting equipment perspective, this approaches basically means putting the hoist cable in slack mode which destroys one of the biggest benefits of the VP over impact hammering piling method and that is the controlled penetration to avoid risk of pile run. Besides that, operational challenges such as inclination of the pile might occur if the piling is not taking place with help of MP gripper. These reasons suffice not to approach this solution for elimination of the hoist cable force.

The second approach, however, is more complex and requires a way to mitigate the hoist cable force while to cause problematic force or vibration in other components.

The idea of an isolator to mitigate the force and vibration is tied to the fact that one or more components to be added to the already built system.

The addition of the isolator can in general bring mass, spring stiffness, and damping coefficient to the system. Before discussing what form of isolator with what kind of component should be selected it is crucial to address where in system this isolator can be placed since the different location of components lead to different results as well.

From practical point of view, it quickly come to realizations that the addition of the isolator is only achievable if is placed below the connection point of the lifting equipments which is the lower block. That is because attachment of the isolator above the hook means either changing the design of the crane which is not desired from the perspective of crane manufacturer who has already built the crane.

And also, attachment of the group of component so called isolator below the bias mass is not feasible. Bias mass and the exciter block, as showed in Fig. 2.4, are two part of the VH with elastomers built in in between. And the exciter block is also connected rigidly to the pile via clamping system.

This left no room for the placement of the isolator other than in between the lower block and the bias mass where the rigging as spring component is. So, putting the isolator in between the lower block and bias mass requires the change in the connections as well.

Now back to the components needed for the isolator. by removing the rigging and placing the mass of the isolator as m_{iso} in between, the rigging as k_3 can be reattached to the m_{iso} at either sides. meaning that the only component representative is the isolator is a discrete mass. However, from the literature it was understood that the lower stiffness the less vibration transfer. This brings us to the option of introducing a new connection instead of using the same or ever shorter rigging cable with higher stiffness.

This new stiffness called k_{iso} now can either be attached to the lower block making the isolator or attached to the bias mass. It is worth noting that rigging as a cable still has to be existed because this component has a crucial role in operational procedure allowing the room for on site engineers and operators to connect lifting equipments to the piling equipments with ease.

That being said, the m_{iso} should be connected to lower block and bias mass with two connections of k_3 and k_{iso} but which of these to connections connects the m_{iso} to the lower block and which con-

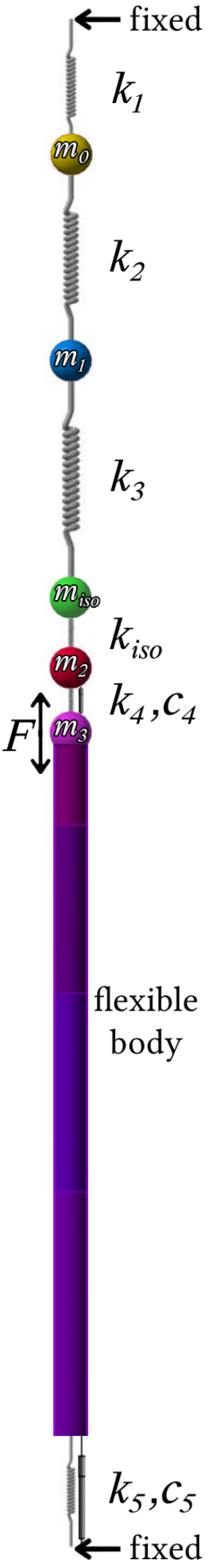

Figure 7.1: Harmonic response analysis model with addition of isolator

nects the m_{iso} to the bias mass still has to be determined.

Either ways have been tested and proved to be effective in reducing the hoist cable force but the connection of m_{iso} to the bias mass via k_{iso} proved to be more effective and this configuration will be evaluated from now on.

The addition of damping to the isolator is still a matter of discussion but for now, it would not be included to the isolator, so the effectiveness of the isolator will be checked purely based on the mass and spring (m_{iso} and k_{iso}).

7.1. Isolator Specifications

To specify the parameters of the isolator as m_{iso} and k_{iso}, it is first essential to understand what are the lower and upper bounds of each parameter. The value for these two parameters and their bounds will be investigated individually in the following subsections.

7.1.1. Stiffness of Isolator

In theory, the stiffness of the isolator can range from zero to infinitely large, effectively making the connection of m_{iso} to the bias mass rigid. However, the literature indicates that lower stiffness results in better isolation. Therefore, the most effective isolator would ideally have a very small stiffness. In practice, however, achieving extremely low stiffness is not feasible, as it leads to large displacements. If the isolator is implemented as a spring, very small stiffness would cause it to deform to its maximum deflection stroke.

Determining the minimum achievable stiffness is a complex topic that requires a separate study and will not be investigated in this research. In this study, the stiffness of the isolator is taken as the minimum available stiffness in the model without the isolator, namely, the stiffness of the elastomers. Among the components, k_4 has the lowest stiffness and is therefore assumed to represent the stiffness of the isolator (k_{iso}).

7.1.2. Mass of Isolator

Determining the minimum and maximum mass of the isolator is straightforward. Theoretically, this mass can be very small at its lower bound, meaning it has practically no mass-related effect compared to the other heavy components of the system. However, it cannot be extremely large due to the lifting capacity of the crane, which in this case is metric tons. This means that the total weight of all components cannot exceed the safe working load (SWL).

Therefore, m_{iso} can range from a small mass relative to the other components, such as 1 ton, up to 2705 tons, which is the maximum payload that can be added to the crane before exceeding its safe working load. It is evident that neither extreme is practical or achievable, but for the purpose of identifying the pattern of eigenfrequency changes in the system, the stiffness of the isolator (k_{iso}) will be kept constant at $k_{iso} = 66$ kN/mm, while different values of m_{iso} will be tested as listed in Table 7.1 for a depth of 20 m as follows:

Table 7.1: Sensibility of the isolator mass at depth 20 m and isolator stiffness of 66 kN/mm - Eigenfrequencies from modal analysis

m_{iso} **[t]**	**1**	**40**	**54**	**81**	**2700**
	Frequency [Hz]				
Mode 1	1.76	1.75	1.75	1.74	0.73
Mode 2	3.64	3.25	3.12	2.92	1.84
Mode 3	6.69	6.40	6.32	6.21	5.75
Mode 4	7.32	7.22	7.21	7.16	7.15
Mode 5	**23.30**	**23.30**	**23.30**	**23.30**	17.28
Mode 6	157.05	29.7	26.93	24.03	**23.30**

Table 7.1 shows the eigenfrequencies of the system after the implementation of m_{iso} and k_{iso} in the configuration depicted in Fig. 7.1. This table presents the eigenfrequencies obtained from the modal analysis of the newly constructed model, where the isolator stiffness is kept constant and the isolator mass is varied.

It can be observed from Table 7.1 that increasing m_{iso} decreases the eigenfrequencies of all modes except for the mode corresponding to the flexible body natural frequency of the pile, which is mode 5 for all isolator mass variations except the last one. At $m_{iso} = 2700\ t$, mode 6 becomes the flexible body natural frequency, as the previous mode shifts below the pile's flexible body natural frequency.

It can also be inferred from the table that when m_{iso} exceeds 81 t, modes 5 and 6 become closer, reproducing the same issue discussed in Chapter 6.2.1, where resonance affects components with large displacements other than the MP toe. To avoid this issue, it is best to select k_{iso} such that the mode not corresponding to the flexible body natural frequency of the pile remains beyond the operational frequency range of 25 Hz.

According to Table 7.1, $m_{iso} = 54\ t$ or less is preferable. However, as mentioned earlier, the isolator mass cannot approach zero, since in practice, an element with stiffness similar to elastomers possesses a finite weight.

Therefore, the isolator parameters selected for the harmonic analysis are $k_{iso} = 66$ kN/mm and $m_{iso} = 54\ t$.

7.2. Harmonic Response Analysis

The harmonic response analysis of the system with the isolator can reveal the effectiveness of the isolator in eliminating the forces in the hoist cable and reducing the displacements of other components.

For the sake of reproducibility of the new system, the parameters and variables are listed as follows:

Table 7.2: List of Parameters and Variables of the System with Isolator (Approximated Values)

Mass	Value	Unit
m_0	2000	t
m_1	100	t
m_iso	54	t
m_2	100	t
m_3	250	t
Stiffness		
k_1	300	kN/mm
k_2	Table [6.2]	kN/mm
k_3	1000	kN/mm
k_{iso}	66	kN/mm
k_4	60	kN/mm
k_5	Fig. [6.3]	kN/mm
Damping		
c_4	Equation 4.24	kNs/mm
c_5	Fig. [6.3]	kNs/mm

To enable comparison of the harmonic response analysis results with the system without the isolator, the depth selected for determining the depth-dependent parameters should be the same as that used for the system without the isolator, which was 20 m.

The results of the component displacements from the FRF analysis are shown in Fig. 7.2. It should be noted that other depths were also analyzed and exhibited similar behavior to the 20 m case.
In both the simulation and Fig. 7.2, the frequency range has been extended to 30 Hz. This is because the main purpose of the isolator is to shift the mode shape that was previously close to the flexible

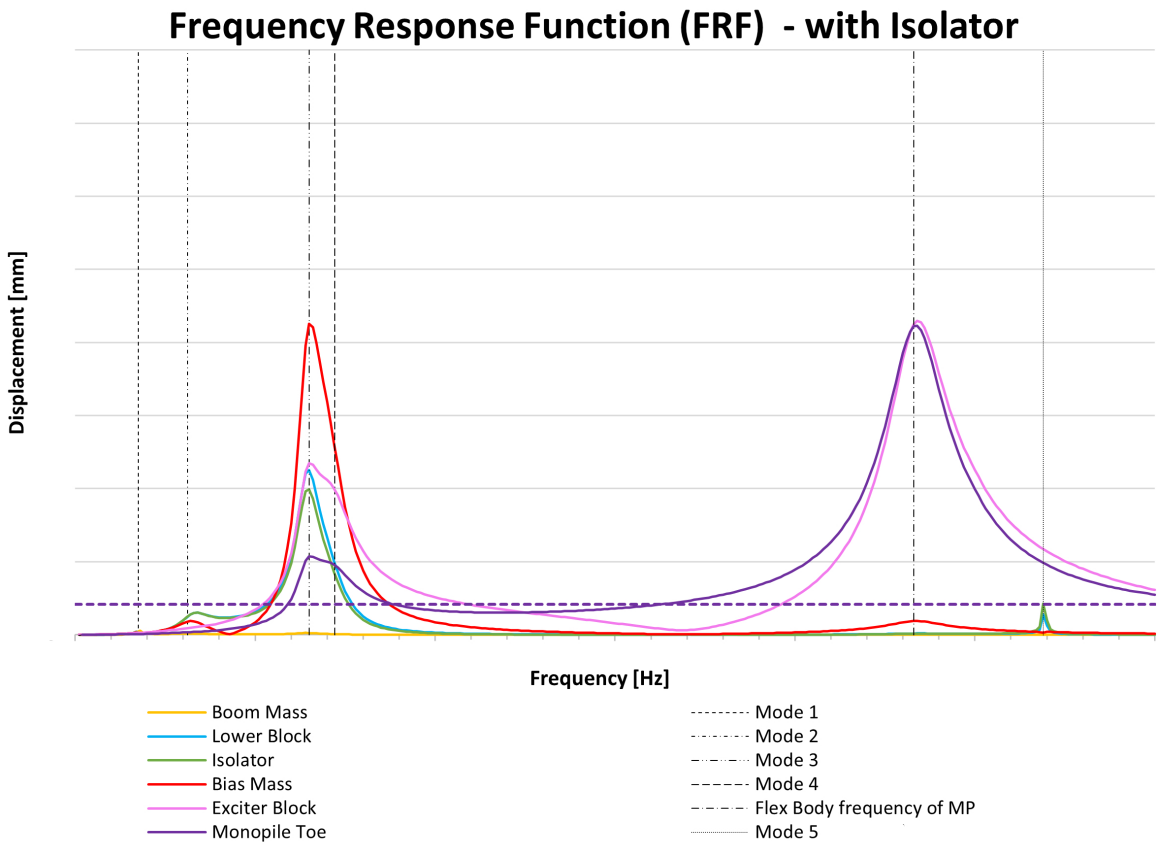

Figure 7.2: Absolute maximum displacement of all the components after the implementation of the isolator in frequency domain

body natural frequency of the pile so that it occurs beyond 25 Hz. As predicted by the modal analysis, the eigenfrequencies corresponding to the peaks are consistent with those listed in Table 7.1 for $m_{iso} = 54\ t$.

In this figure, five peaks can be observed—four corresponding to the four DOF and one representing the flexible body natural frequency of the pile. The maximum displacement of the isolator is shown with a green line, while the other components are depicted in the same colors as in Fig. 6.10.

By comparing Fig. 6.10 and Fig. 7.2, the effect of the isolator becomes evident.

The first notable difference is that the large displacement peaks associated with the lower block and bias mass at 23.01 Hz have disappeared. However, larger displacements for these components now appear at a lower frequency of 6.32 Hz.

8

Discussion

This chapter interprets the analysis results and evaluates the reliability of the adopted modelling choices. The first section explains what the modes imply for the crane, rigging, and MP, and why certain frequencies within the operational band of the VH are critical. The second section outlines the limits of the simplified model and the basis for confidence through comparison with the full FE model. Together, these points set up a concise transition to the conclusions that follow.

8.1. Interpretation of results

The analysis separates two interacting dynamics. First are the system resonance frequencies of the boom mass, lower block, and VH when the MP is treated as rigid. Second is the axial flexible body natural frequency of the MP obtained from the shell model after mode reduction. Modes 1, 2, and 4 show limited sensitivity to MP flexibility, whereas Mode 3 and the axial flexible body frequency depend strongly on toe soil stiffness. The harmonic response confirms this structure. Displacement peaks occur at the eigenfrequencies, and the mode shapes explain which components dominate each peak. Within the operational band of the VH, the fourth system resonance and the first axial flexible body frequency of the MP lie close together and can change order with depth.

For the lifting equipment, the simplified 1D system captures the dominant low frequency global behavior and reproduces the first boom tip peak. In the full FE model, additional peaks appear that are absent from the simplified system. These originate from flexibility in the boom and mast that is activated by force transmitted through the hoist line. Near the fourth resonance, the lower block exhibits the largest motions among the lifting components, which implies elevated alternating loads in sheaves, pins, and wire terminations. At the MP axial flexible body frequency, motion concentrates in the exciter and pile, with secondary effects entering the lifting line and the lower block. The overlap between the efficient penetration band and these two peaks explains the heightened responses observed at several depths.

8.2. Limits and confidence

The modeling choices are deliberate and aligned with the objectives. The pedestal is treated as fixed over the time scale considered. The simplified system is linear with small displacements. Elastomer and soil behavior are represented by depth dependent linear coefficients. Soil is included through a toe spring and damper, and shaft friction is not modeled. The VH input is a single harmonic for each frequency interval. The MP shell contributes only the axial flexible body frequency after mode reduction; bending, torsion, and circumferential shell modes are excluded by design. These choices are suitable for locating resonances, understanding component participation, and estimating wire forces, but they are not intended for stress verification or fatigue assessment.

Direct field measurements are not yet available. As a surrogate, the simplified system was compared with a detailed full FE crane model under identical boundary conditions and inputs. The first boom tip peak is captured in both, which supports the simplified system for global low frequency behavior. Additional peaks in the full FE model are traced to flexibility of boom and mast substructures that the simplified system does not represent. This comparison clarifies which conclusions are robust and which depend on local crane flexibility. With this context established, the next chapter summarizes the main findings in relation to the research objectives.

8.3. Solution intervals sensitivity

The number of solution intervals sets the frequency resolution of the harmonic response and, therefore, how finely the peaks are sampled. In this study, the range 0–25 Hz was discretized into 200 intervals (0.125 Hz steps) and, when the isolator was included, 0–30 Hz into 300 intervals (0.10 Hz steps). These choices balanced run time and curve smoothness, and because the exact peak locations were known from the modal analysis, they were sufficient to capture the resonance bands without missing them.

Sensitivity tests showed that increasing the number of intervals can yield larger peak amplitudes for the isolator and equivalent boom mass components. This behavior is expected for lightly damped or undamped models; as damping tends to zero, the frequency response near resonance becomes very sharp, and a finer grid samples points closer to the singular peak, producing higher reported magnitudes. In the present setups, the equivalent boom mass element and the added isolator do not include damping, so peak estimates are resolution-dependent. Practically, this is acceptable for two reasons: first, during ramp-up the vibratory hammer sweeps through the frequency range of 0-15 Hz rapidly. Second, the largest undamped peak for the isolator sits outside the operational band and will never be reached.

For completeness, future isolator design and validation should incorporate damping in the isolator design (and, if applicable, in equivalent and simplified crane components) to regularize the peaks and reduce sensitivity to the chosen frequency resolution. Adaptive refinement of the frequency grid in narrow windows around the eigenfrequencies would further ensure consistent peak capture at reasonable computational cost.

9

Conclusion

This chapter distills the essential findings of the study into clear statements and answers the research questions. The conclusions are based on the simplified system model and on comparisons with the full FE model under consistent inputs and boundary conditions.

Key conclusions

- The dynamic response is governed by two frequency families: the system resonances with the MP treated as rigid, and the axial flexible body natural frequency of the MP obtained after mode reduction. Within the operational range of the VH, the fourth system resonance and the first axial flexible body frequency are the decisive pair.
- Depth dependent soil stiffness shifts Mode 3 and the MP axial frequency, which explains the observed movement of the dominant peaks with penetration depth. Modes 1, 2, and 4 are comparatively insensitive to MP flexibility.
- The simplified 1D system, which idealizes the boom and mast as rigid, reproduces the first boom tip peak and captures the low frequency global behavior that matters for initial validation.
- Discrepancies at higher frequencies between the simplified system and the full FE model arise from flexibility of the boom and mast that is excited by force transmitted through the hoist line. The source of the difference is therefore the crane structure itself, not the modeling of the piling equipment.
- The hoist cable force predicted by the simplified system agrees with the full FE model over the investigated range because the harmonic input is generated in the piling equipment. The magnitude and trend are controlled by elastomer and soil properties and by hoist stiffness, not by whether the boom and mast are modeled as flexible or rigid.
- An isolator inserted in the load path acts as a mechanical filter in the vicinity of the MP axial frequency. With appropriate tuning, it reduces force transmission into the boom and lowers boom tip motion while preserving the drivability benefits of the VH.
- The necessity of adding an isolator can be justified in cases where a mode associated with unwanted vibrations of the lower block falls within the operational frequency range. If the operational frequency range is already free of disruptive modes for the lifting equipment, adding an isolator may instead introduce undesirable vibration modes with larger displacements in other system components.

Answers to the research questions

Primary question. *What risks are posed to the lifting equipment during VP due to vibration transmission?*

The lifting equipment is exposed to elevated alternating loads when the input frequency is near the fourth system resonance or near the MP axial flexible body frequency. The lower block is the most affected lifting component at the fourth resonance, and boom tip motion increases in the detailed crane when hoist force excites flexible modes of the boom and mast. These effects represent credible risks to sheaves, pins, wire terminations, and boom structural details.

Sub question 1. *What is the force in the hoist cable introduced by the VH?*

The computed hoist cable force from the simplified system matches the full FE model. Its level and variation are set by the vibratory input and by depth dependent elastomer and soil properties, not by crane structural flexibility.

Sub question 2. *What are the resonance frequencies of the system?*

With a rigid MP, four resonance frequencies are present and can be obtained from the system matrices. When MP flexibility is included, the first axial flexible body frequency appears in addition to those four. The fourth resonance and the axial frequency fall inside the operational range of the VH, and their relative order can change with depth.

Sub question 3. *How does each system component behave with respect to the input frequency of the VH?*

Component participation is mode specific. Modes 1 and 2 are dominated by boom mass and by the pair of lower block and bias mass. Mode 3 is governed by exciter and MP, with strong soil engagement. Mode 4 concentrates motion in the lower block and bias mass with limited MP response. At the MP axial frequency the head and toe move in opposite directions with a near stationary point along the pile axis, consistent with a fundamental axial mode.

Sub question 4. *What are the displacement magnitudes of the system components?*

Harmonic response results provide absolute displacement magnitudes over frequency. The largest lifting equipment displacements occur near the fourth resonance, and the largest MP elongation occurs at the MP axial frequency.

Secondary question. *Do the input frequencies that are most effective for pile penetration also pose risks for the lifting equipment?*

Yes. The efficient penetration band overlaps with the fourth system resonance and the MP axial frequency at several depths. Operation in these bands increases lower block motion, hoist force fluctuation, and, in the detailed crane, boom tip response. Managing these risks requires avoiding narrow bands around the peaks where practicable, controlling hoist tension, and using isolation to reduce transmission into the crane.

10

Future Research

This study delivers a first system view of vibration transmission during VP, but several gaps remain before the results can serve as a predictive, field validated basis for design and operations. The following four priorities would add the most value.

1. Measurement driven validation

Plan instrumented campaigns during VP to record boom tip motion, lower block motion, hoist tension, exciter force, and MP head and toe motion, synchronised with VH control signals. Derive operating deflection shapes and empirical frequency response functions to identify modal parameters and calibrate soil and elastomer properties. These measurements are essential to confirm which peaks dominate in practice and to bound model uncertainty.

2. Soil and structural coupling at system level

Extend the model to include distributed shaft resistance and damping along the embedded length, and allow stiffness and damping to vary with depth and strain level. Replace the rigid boom and mast in the simplified system with reduced order flexible representations traceable to the full FE model. This will capture the additional peaks seen only in the detailed crane and quantify how soil trends with depth shift Mode 3 and the MP axial flexible body frequency.

3. Crane and pile fatigue damage

Investigate the potential risk of fatigue and life-span reduction in both crane components and the pile resulting from sustained high-frequency vibrations. This should include detailed stress analysis of critical crane parts as well as the pile shaft and toe. Fatigue life estimation methods, such as rainflow counting or Miner's rule, can be applied using simulated or measured stress histories. Additionally, assess how varying excitation frequencies and isolator configurations influence cyclic loading patterns, enabling the development of design guidelines to mitigate long-term damage.

4. Isolation concept design and tuning

Develop and compare isolation concepts placed between the lifting equipment and the piling equipment. Optimize their parameters to reduce force transmission near the fourth system resonance and the MP axial flexible body frequency while preserving penetration efficiency. Produce simple selection and tuning charts that relate isolator settings to expected reductions in hoist force fluctuation and boom tip response.

Bibliography

Arany, L., Bhattacharya, S., Macdonald, J., & Hogan, S. J. (2017). Design of monopiles for offshore wind turbines in 10 steps. *Soil Dynamics and Earthquake Engineering*, *92*, 126–152.

BOSLAN Ingeniería Consultoría. (2022). *Xxl monopiles: Analysis of current state and future perspectives* (tech. rep.) (States diameters up to 11 m and lengths up to 120 m). https://www.boslan.com/offshore-wind-farms/monopile-foundations-mb/

Fayat group vh [Accessed: 2025-10-22]. (n.d.).

Feng, Z., & Deschamps, R. J. (2000). A study of the factors influencing the penetration and capacity of vibratory driven piles. *Soils and foundations*, *40*(3), 43–54.

Gazetas, G. (1991). Foundation vibrations. In *Foundation engineering handbook* (pp. 553–593). Springer.

Gazetas, G., & Makris, N. (1991). Dynamic pile-soil-pile interaction. part i: Analysis of axial vibration. *Earthquake Engineering & Structural Dynamics*, *20*(2), 115–132.

International Crane Stakeholder Assembly (ICSA). (2022, April). *Using mobile cranes with freely suspended vibratory equipment for pile driving / extraction* (tech. rep. No. ICSA N006) (Initial release edited by FEM, approved 12 April 2022). International Crane Stakeholder Assembly (ICSA). Frankfurt, Germany. https://www.icsa-crane.org

J&m model 14412t. (2025). https://www.americanpiledriving.com/specifications/JnM/JM_VIBRO_1412T.pdf

Kallehave, D., Byrne, B. W., LeBlanc Thilsted, C., & Mikkelsen, K. K. (2015). Optimization of monopiles for offshore wind turbines. *Philosophical Transactions of the Royal Society A: Mathematical, Physical and Engineering Sciences*, *373*(2035), 20140100.

Lee, S.-H., Kim, B.-I., & Han, J.-T. (2012). Prediction of penetration rate of sheet pile installed in sand by vibratory pile driver. *KSCE Journal of Civil Engineering*, *16*, 316–324.

Leissa, A. W. (1973). Vibration of shells (nasa sp-288). *Washington, DC: US Government Printing Office*.

LLC, D. O. U., & Inc., R. G. (2024, April). *Pile driving monitoring, mitigation and management plan: Coastal virginia offshore wind commercial project* (tech. rep. No. CVOW1-TIP-DMN-PLN-EN-00004) (Prepared for Dominion Energy, Richmond, VA. Revision 03, Approved May 3, 2024). DEME Offshore US LLC. East Boston, MA. URL_if_available

Massarsch, K. R., Fellenius, B. H., & Bodare, A. (2017). Fundamentals of the vibratory driving of piles and sheet piles. *geotechnik*, *40*(2), 126–141.

McCoy, A., Musial, W., Hammond, R., Mulas Hernando, D., Duffy, P., Beiter, P., Perez, P., Baranowski, R., Reber, G., & Spitsen, P. (2024). *Offshore wind market report: 2024 edition* (tech. rep.). National Renewable Energy Laboratory (NREL), Golden, CO (United States).

Niu, F., Xie, J., Zhang, X., Xue, R., Chen, B., Liu, Z., & Yang, Y. (2023). Assessing differences in acoustic characteristics from impact and vibratory pile installation and their potential effects on the large yellow croaker (pseudosciaena crocea). *Frontiers in Marine Science*, *10*, 1106980.

Novak, M. (1977). Vertical vibration of floating piles. *Journal of the Engineering Mechanics Division*, *103*(1), 153–168.

Offshore vibro piling. (2023). https://www.tudelftcampus.nl/time-to-shake-up-the-pile-driving-industry/#

Rainer Massarsch, K., Wersäll, C., & Fellenius, B. H. (2022). Vibratory driving of piles and sheet piles–state of practice. *Proceedings of the Institution of Civil Engineers-Geotechnical Engineering*, *175*(1), 31–48.

Rodger, A., & Littlejohn, G. (1980). A study of vibratory driving in granular soils. *Geotechnique*, *30*(3), 269–293.

Seiche Ltd. (2021). *Review of underwater sound from piling and other offshore construction and maintenance activities* (tech. rep.) (Summarizes that vibratory piling produces lower peak sound levels than impact piling). https://www.seiche.com/wp-content/uploads/2020/10/Review_on_Pile_Driving.pdf

Tsetas, A., Tsouvalas, A., & Metrikine, A. V. (2023). The mechanics of the gentle driving of piles. *International Journal of Solids and Structures*, *282*, 112466.

Tsouvalas, A., de Roo, C., Renting, F., & Hengeveld, F. (n.d.). Sustainable installation of xxl monopiles.

Viking, K. (2002). *Vibro-driveability-a field study of vibratory driven sheet piles in non-cohesive soils* [Doctoral dissertation, Byggvetenskap].

Warrington, D. C. (1992). Vibratory and impact-vibration pile driving equipment. *Pile Buck (Second Issue), 2A–28A*.

Whenham, V. (2011). *Power transfer and vibrator-pile-soil interactions within the framework of vibratory pile driving* [Doctoral dissertation, University of Louvain Leuven, Belgium].

Whenham, V., & Holeyman, A. (2012). Load transfers during vibratory driving. *Geotechnical and Geological Engineering*, *30*, 1119–1135.

A

Appendix

A.1. Solver Outputs

A.1.1. Participation Factor at depth 20 meters

Participation Factor

Mode	Frequency [Hz]	X Direction	Y Direction	Z Direction	Rotation X	Rotation Y	Rotation Z
1	1.8011282	6.4535396e-015	3.4365519e-016	45.437138	-3.0341037e-010	-3.0300357e-010	-5.1017697e-011
2	3.7038624	3.429177e-014	-1.1325621e-015	13.748305	-7.5891345e-010	-1.5695033e-009	6.2360966e-011
3	4.682085	36.760589	0.15905964	7.3835224e-015	8229.7457	-1901992.9	1.6514113e-007
4	4.682085	-0.15905964	36.760589	-1.69264e-015	1901992.9	8229.7457	6.1937064e-008
5	5.9615853	-1.9910187e-014	-2.1500786e-015	44.0762	-8.7341381e-010	1.6208653e-009	-7.6281727e-012
6	11.568105	5.0093263e-013	7.3240025e-015	-3.1384372e-014	1121.5973	910981.25	-1.2048234e-009
7	11.568105	3.5388359e-016	7.5672801e-013	-3.8619641e-014	-910981.25	1121.5973	-1.0854357e-010
8	15.125408	-3.2684982e-011	-1.2479718e-011	1.2327016e-014	-6.4708121e-007	1.697079e-006	172905.17
9	20.273288	16.687746	1.3690947e-002	3.1810631e-015	708.3696	-863423.97	-1.8663608e-008
10	20.273288	-1.3690947e-002	16.687746	3.0782423e-014	863423.97	708.3696	-7.2425126e-009
11	23.028198	3.7015031e-014	-9.1450322e-016	0.60366868	4.9540209e-011	-1.2443191e-009	-6.6675446e-011
12	23.649056	3.3106383e-015	3.4435318e-014	4.9787653	1.7332331e-009	-5.3168252e-011	-4.6215662e-010
13	30.021953	2.4424907e-013	-1.3062728e-013	5.3334397e-014	339.50792	-593616.13	4.1835029e-011
14	30.021953	-5.3641119e-014	-1.2612134e-013	-2.6141372e-014	-593616.13	-339.50792	1.4191265e-010
15	30.250822	9.0711496e-015	1.128388e-013	7.9715566e-016	-4.3359699e-007	1.48442e-006	1.9790605e-009
16	40.41831	10.404348	-6.7292963e-004	-3.4485859e-014	-34.817379	-538320.98	3.8833805e-009
17	40.41831	6.7292963e-004	10.404348	-7.7741569e-015	538320.98	-34.817379	2.1779026e-009
18	44.945956	-2.5014422e-014	-7.0171851e-016	-1.4847645	-4.0333057e-010	1.0319379e-009	8.4760831e-011
19	45.376277	2.1695835e-012	9.8818422e-013	-2.7976712e-014	4.5625888e-008	-1.0953181e-007	-57635.197
20	51.211009	5.6665783e-013	-4.0128924e-014	-2.7111189e-014	209.26587	-416438.89	-4.8679931e-010
21	51.211009	-8.7456518e-014	7.2741813e-013	1.9784652e-014	416438.89	209.26587	-3.7759042e-010
22	60.501862	-2.6995012e-013	4.2783481e-013	-5.5414424e-014	4.6344472e-009	5.3274893e-008	1.8262654e-009
23	62.24051	7.2114366	-3.7779147e-003	6.362422e-015	-195.4693	-373119.73	4.0660018e-010
24	62.24051	3.7779147e-003	7.2114366	-1.3282052e-014	373119.73	-195.46931	2.7404121e-010
25	67.393797	8.6073836e-014	2.8097325e-014	0.67795672	-8.7435434e-010	-5.1104482e-009	3.471298e-010
26	73.398725	-9.7033492e-013	1.5951216e-014	8.0848249e-015	341.25799	308339.23	1.0266419e-010
27	73.398725	1.6796785e-013	-1.2696511e-012	-3.3340098e-014	-308339.23	341.25799	1.3682341e-009
28	75.627747	-3.4968172e-013	-2.1141526e-013	7.4346951e-014	-4.4565262e-010	1.6167151e-008	34581.684
29	84.616301	5.3602425	-4.0640079e-003	4.7259755e-014	-210.27177	-277338.95	-2.5821579e-009
30	84.616301	4.0640079e-003	5.3602425	-4.9578919e-014	277338.95	-210.27177	3.9651799e-009

Figure A.1: Participation factor table for the first 30 modes of the system at penetration depth of 20 meters

A.1.2. Effective Mass at depth 20 meters

Effective Mass

Mode	Frequency [Hz]	X Direction [tonne]	Y Direction [tonne]	Z Direction [tonne]	Rotation X [tonne mm mm]	Rotation Y [tonne mm mm]	Rotation Z [tonne mm mm]
1	1.8011282	4.1648173e-029	1.1809889e-031	2064.5335	9.2057854e-020	9.1811162e-020	2.6028054e-021
2	3.7038624	1.1759255e-027	1.282697e-030	189.0159	5.7594963e-019	2.4633405e-018	3.88889e-021
3	4.682085	1351.3409	2.5299969e-002	5.4516403e-029	67728714	3.617577e+012	2.7271594e-014
4	4.682085	2.5299969e-002	1351.3409	2.8650301e-030	3.617577e+012	67728714	3.8361999e-015
5	5.9615853	3.9641553e-028	4.622838e-030	1942.7114	7.6285169e-019	2.6272043e-018	5.8189019e-023
6	11.568105	2.509335e-025	5.3641013e-029	9.849788e-028	1257980.6	8.2988683e+011	1.4515995e-018
7	11.568105	1.2523359e-031	5.7263729e-025	1.4914767e-027	8.2988683e+011	1257980.6	1.1781708e-020
8	15.125408	1.0683081e-021	1.5574336e-022	1.5195533e-028	4.1871409e-013	2.8800771e-012	2.9896199e+010
9	20.273288	278.48086	1.8744203e-004	1.0119162e-029	501787.49	7.4550095e+011	3.4833027e-016
10	20.273288	1.8744203e-004	278.48086	9.4755759e-028	7.4550095e+011	501787.49	5.2453988e-017
11	23.028198	1.3701125e-027	8.3631614e-031	0.36441587	2.4542323e-021	1.54833e-018	4.4456151e-021
12	23.649056	1.0960326e-029	1.1857911e-027	24.788104	3.0040971e-018	2.826863e-021	2.1358874e-019
13	30.021953	5.9657606e-026	1.7063486e-026	2.8445579e-027	115265.63	3.5238011e+011	1.7501696e-021
14	30.021953	2.8773697e-027	1.5906591e-026	6.8337135e-028	3.5238011e+011	115265.63	2.0139201e-020
15	30.250822	8.2285755e-029	1.2732594e-026	6.3545714e-031	1.8800635e-013	2.2035027e-012	3.9166803e-018
16	40.41831	108.25046	4.5283428e-007	1.1892745e-027	1212.2499	2.8978948e+011	1.5080644e-017
17	40.41831	4.5283428e-007	108.25046	6.0437516e-029	2.8978948e+011	1212.2499	4.7432597e-018
18	44.945956	6.257213e-028	4.9240886e-031	2.2045255	1.6267555e-019	1.0648958e-018	7.1843984e-021
19	45.376277	4.7070926e-024	9.7650806e-025	7.8269644e-028	2.0817217e-015	1.1997217e-014	3.3218159e+009
20	51.211009	3.211011e-025	1.6103306e-027	7.3501658e-028	43792.202	1.7342135e+011	2.3697356e-019
21	51.211009	7.6486425e-027	5.2913713e-025	3.9143245e-028	1.7342135e+011	43792.202	1.4257453e-019
22	60.501862	7.2873065e-026	1.8304262e-025	3.0707584e-027	2.1478101e-017	2.8382142e-015	3.3352452e-018
23	62.24051	52.004818	1.4272639e-005	4.0480414e-029	38208.249	1.3921833e+011	1.6532371e-019
24	62.24051	1.4272639e-005	52.004818	1.764129e-028	1.3921833e+011	38208.249	7.5098585e-020
25	67.393797	7.4087053e-027	7.8945968e-028	0.45962532	7.6449552e-019	2.6116681e-017	1.204991e-019
26	73.398725	9.4154986e-025	2.5444129e-028	6.5364394e-029	116457.02	9.5073081e+010	1.0539935e-020
27	73.398725	2.82132e-026	1.6120138e-024	1.1115621e-027	9.5073081e+010	116457.02	1.8720645e-018
28	75.627747	1.2227731e-025	4.4696413e-026	5.5274691e-027	1.9860626e-019	2.6137677e-016	1.1958928e+009
29	84.616301	28.7322	1.651616e-005	2.2334844e-027	44214.217	7.6916891e+010	6.6675396e-018
30	84.616301	1.651616e-005	28.7322	2.4580692e-027	7.6916891e+010	44214.217	1.5722652e-017
Sum		1818.8348	1818.8348	4224.0775	6.3198338e+012	6.3198338e+012	3.4413908e+010

Figure A.2: Effective mass table for the first 30 modes of the system at penetration depth of 20 meters

A.1.3. Cumulative Effective Mass Fraction at depth 20 meters

Cumulative Effective Mass Fraction

Mode	Frequency [Hz]	X Direction	Y Direction	Z Direction	Rotation X	Rotation Y	Rotation Z
1	1.8011282	2.2898272e-032	6.4931069e-035	0.4887537	1.4566499e-032	1.4527465e-032	7.563237e-032
2	3.7038624	6.6942512e-031	7.7016116e-034	0.53350096	1.0570017e-031	4.0430678e-031	1.8863581e-031
3	4.682085	0.74297068	1.3909987e-005	0.53350096	1.0716851e-005	0.57241647	7.9245869e-025
4	4.682085	0.74298459	0.74298459	0.53350096	0.57242718	0.57242718	9.0393106e-025
5	5.9615853	0.74298459	0.74298459	0.99341473	0.57242718	0.57242718	9.0393106e-025
6	11.568105	0.74298459	0.74298459	0.99341473	0.57242738	0.70374184	9.0397324e-025
7	11.568105	0.74298459	0.74298459	0.99341473	0.70374204	0.70374204	9.0397358e-025
8	15.125408	0.74298459	0.74298459	0.99341473	0.70374204	0.70374204	0.86872433
9	20.273288	0.89609408	0.7429847	0.99341473	0.70374212	0.82170416	0.86872433
10	20.273288	0.89609418	0.89609418	0.99341473	0.82170424	0.82170424	0.86872433
11	23.028198	0.89609418	0.89609418	0.99350101	0.82170424	0.82170424	0.86872433
12	23.649056	0.89609418	0.89609418	0.99936929	0.82170424	0.82170424	0.86872433
13	30.021953	0.89609418	0.89609418	0.99936929	0.82170425	0.87746205	0.86872433
14	30.021953	0.89609418	0.89609418	0.99936929	0.87746207	0.87746207	0.86872433
15	30.250822	0.89609418	0.89609418	0.99936929	0.87746207	0.87746207	0.86872433
16	40.41831	0.95561057	0.89609418	0.99936929	0.87746207	0.92331604	0.86872433
17	40.41831	0.95561057	0.95561057	0.99936929	0.92331604	0.92331604	0.86872433
18	44.945956	0.95561057	0.95561057	0.99989119	0.92331604	0.92331604	0.86872433
19	45.376277	0.95561057	0.95561057	0.99989119	0.92331604	0.92331604	0.96524972
20	51.211009	0.95561057	0.95561057	0.99989119	0.92331605	0.95075685	0.96524972
21	51.211009	0.95561057	0.95561057	0.99989119	0.95075685	0.95075685	0.96524972
22	60.501862	0.95561057	0.95561057	0.99989119	0.95075685	0.95075685	0.96524972
23	62.24051	0.98420295	0.95561057	0.99989119	0.95075686	0.97278565	0.96524972
24	62.24051	0.98420295	0.98420295	0.99989119	0.97278566	0.97278566	0.96524972
25	67.393797	0.98420295	0.98420295	1.	0.97278566	0.97278566	0.96524972
26	73.398725	0.98420295	0.98420295	1.	0.97278567	0.98782926	0.96524972
27	73.398725	0.98420295	0.98420295	1.	0.98782928	0.98782928	0.96524972
28	75.627747	0.98420295	0.98420295	1.	0.98782928	0.98782928	1.
29	84.616301	0.99999999	0.98420296	1.	0.98782929	0.99999999	1.
30	84.616301	1.	1.	1.	1.	1.	1.

Figure A.3: Cumulative effective mass fraction table for the first 30 modes of the system at penetration depth of 20 meters

A.1.4. Ratio of Effective Mass to Total Mass at depth 20 meters

Ratio of Effective Mass to Total Mass

Mode	Frequency [Hz]	X Direction	Y Direction	Z Direction	Rotation X	Rotation Y	Rotation Z
1	1.8011282	9.8586574e-033	2.7955523e-035	0.48870158	1.2665199e-032	1.263126e-032	7.056933e-032
2	3.7038624	2.7835667e-031	3.0363086e-034	4.474249e-002	7.9238398e-032	3.3890317e-031	1.0543868e-031
3	4.682085	0.31987975	5.9888275e-006	1.2904733e-032	9.3180281e-006	0.49770152	7.3940913e-025
4	4.682085	5.9888275e-006	0.31987975	6.7818942e-034	0.49770152	9.3180281e-006	1.040101e-025
5	5.9615853	9.3836646e-032	1.0942851e-033	0.45986474	1.0495214e-031	3.6144734e-031	1.577667e-033
6	11.568105	5.9399181e-029	1.2697517e-032	2.3315713e-031	1.7307132e-007	0.11417475	3.9356919e-029
7	11.568105	2.96444e-035	1.355506e-028	3.5305168e-031	0.11417475	1.7307132e-007	3.1943503e-031
8	15.125408	2.5288224e-025	3.6866453e-026	3.5969779e-032	5.7606138e-026	3.9623725e-025	0.81056952
9	20.273288	6.5919995e-002	4.4369936e-008	2.3953357e-033	6.9035268e-008	0.10256505	9.4442072e-027
10	20.273288	4.4369936e-008	6.5919995e-002	2.2429905e-031	0.10256505	6.9035268e-008	1.4221742e-027
11	23.028198	3.2432322e-031	1.9796677e-034	8.6261916e-005	3.3765007e-034	2.1301723e-031	1.2053305e-031
12	23.649056	2.5944499e-033	2.8069198e-031	5.8676624e-003	4.1329976e-031	3.8891612e-034	5.7909878e-030
13	30.021953	1.4121721e-029	4.0391463e-030	6.7334339e-031	1.5858095e-008	4.8479996e-002	4.745199e-032
14	30.021953	6.8111035e-031	3.7652944e-030	1.6176277e-031	4.8479996e-002	1.5858095e-008	5.4603004e-031
15	30.250822	1.9478095e-032	3.0139685e-030	1.5042087e-034	2.5865668e-026	3.0315503e-025	1.0619215e-028
16	40.41831	2.5624275e-002	1.0719169e-010	2.8151655e-031	1.6677976e-010	3.9868858e-002	4.0887841e-028
17	40.41831	1.0719169e-010	2.5624275e-002	1.4306336e-032	3.9868858e-002	1.6677976e-010	1.2860303e-028
18	44.945956	1.4811627e-031	1.165595e-034	5.2183949e-004	2.238069e-032	1.4650697e-031	1.9478912e-031
19	45.376277	1.1142293e-027	2.31152e-028	1.852743e-031	2.8640055e-028	1.6505615e-027	9.0063714e-002
20	51.211009	7.6008753e-029	3.8118593e-031	1.7398786e-031	6.0248741e-009	2.3859083e-002	6.4250157e-030
21	51.211009	1.8105319e-030	1.2525355e-028	9.2657086e-032	2.3859083e-002	6.0248741e-009	3.8655939e-030
22	60.501862	1.724999e-029	4.3328539e-029	7.2688794e-031	2.954929e-030	3.904778e-028	9.0427819e-029
23	62.24051	1.2310208e-002	3.378517e-009	9.5822337e-033	5.2566411e-009	1.9153476e-002	4.4823879e-030
24	62.24051	3.378517e-009	1.2310208e-002	4.1759198e-032	1.9153476e-002	5.2566411e-009	2.0361325e-030
25	67.393797	1.7537357e-030	1.8687524e-031	1.0879921e-004	1.051783e-031	3.5930989e-030	3.2670674e-030
26	73.398725	2.2287694e-028	6.0229521e-032	1.5472591e-032	1.6022004e-008	1.308003e-002	2.8576711e-031
27	73.398725	6.6784267e-030	3.8158436e-028	2.6312103e-031	1.308003e-002	1.6022004e-008	5.0756902e-029
28	75.627747	2.8944608e-029	1.0580215e-029	1.3084229e-030	2.732399e-032	3.5959875e-029	3.2423998e-002
29	84.616301	6.8012806e-003	3.9095872e-009	5.2869444e-031	6.0829342e-009	1.0582125e-002	1.8077564e-028
30	84.616301	3.9095872e-009	6.8012806e-003	5.8185654e-031	1.0582125e-002	6.0829342e-009	4.2628504e-028
Sum		0.43054155	0.43054155	0.99989337	0.86947449	0.86947449	0.93305723

Figure A.4: Ration of effective mass to total mass table for the first 30 modes of the system at penetration depth of 20 meters